Spectroscopic determination of particle fluxes and charge-state distributions in a pulsed-diode plasma

Y. Maron, L. Perelmutter, E. Sarid, M. E. Foord, and M. Sarfaty
Department of Physics, Weizmann Institute of Science, Rehovot 76100, Israel
(Received 27 January 1988; revised manuscript received 13 September 1989)

We have determined the absolute fluxes of various species injected from a dielectric surface into the surface-flashover-produced anode plasma in a magnetically insulated ion diode by observations of time-dependent line intensities and use of time-dependent collisional radiative calculations. Neutral particles, singly charged ions, and doubly charged ions produced on the dielectric surface were found to be continuously injected during the voltage pulse with the injection of neutral particles and singly charged ions continuing also after the main pulse. The determined fluxes explained the observed rise in the areal density of the plasma electrons. Using observed particle velocity distributions the particle flow in the plasma was calculated. It was found that mainly multiply charged ions and protons reach the plasma ion-emitting region. The flux ratio of doubly charged ions to protons produced by hydrogen ionization in the outer plasma region was found to rise towards the end of the pulse, consistent with the corresponding ratio in the extracted ion beam. The determined plasma composition allowed the electron-cooling processes to be evaluated. Such investigations can be used in plasma source design.

I. INTRODUCTION

The behavior of plasmas formed in pulsed power ($\simeq$100-ns) systems is considerably influenced by their time-dependent composition and charge state. These factors affect the plasma density, flow, conductivity, collisionality, and ion extraction from the plasma in the presence of electric fields. Studying the plasma composition is important for the understanding of the operation of pulsed systems as well as for improving the design of plasma sources for various applications.

Determination of the plasma composition in pulsed devices is difficult since the charge states in the plasma change rapidly in time because of particle ionization, and the plasma remains far from ionization equilibrium with the recombination processes playing a negligible role.[1] Furthermore, material usually flows continuously into the plasma throughout the pulse either from the plasma sources used or from surfaces in contact with the plasma.

For the investigation of the ionization processes in such transient plasmas knowledge of the electron density and temperature is essential. Moreover, determining the particle abundances from emission line intensities requires time-dependent calculations of the atomic processes that yield the evolution of the atomic level populations as a function of time. Using steady-state calculations in transient plasmas often can give misleading results since the level populations are mainly determined by excitations from the ground state.[1] It is shown in this paper that for the plasma parameters presently considered, using measured line intensities and steady-state calculations to obtain the total particle density or the total density of the higher-charge-state particles gives results which are in error by several orders of magnitude.

In this study we report on an investigation of the time-dependent composition, charge-state distribution, and spatial particle distribution in the anode plasma in a magnetically insulated ion diode. In intense ion-beam diodes,[2,3] in particular, the spatial particle distribution in the anode plasma determines the extraction of various ion species and charge states into the diode acceleration gap, thus determining the ion-beam composition. The control of the latter is important, to varying degrees, for applications of ion beams in inertial confinement fusion,[3,4] plasma confinement and heating in magnetic confinement fusion,[5] and material science.[6]

A widely used source in intense ion-beam diodes is the surface-flashover-produced plasma.[7] This is a passive source in which the plasma is produced on a dielectric-filled metal anode presumably as a result of an electrical breakdown in neutral desorbed gas released from the dielectric surface.[8] The processes responsible for the plasma formation and the material release from the surface are not addressed in this study.

Subsequent to the plasma formation, the plasma composition and density throughout the pulse are determined by ion losses to the diode acceleration gap and by material flow to and from the dielectric anode surface. It is known[9,10] that ion beams produced from surface-flashover anode plasmas are composed of constituents of both the anode dielectric and surface impurities. The relative abundance of the various species is determined by mechanisms as yet not well understood, related to the surface preparation, the diode vacuum conditions, and the surface flashover processes. The extraction of various ions from the plasma depends on the material ejection from the anode surface into the plasma, the time-dependent ionization processes in the plasma, and the ion flow from the dielectric surface towards the ion-emitting region of the plasma. Measurements of the proton fraction in the generated ion beams indicated large variations (30–80 %) for similar diode configurations.[11–13]

In order to improve the understanding of these complicated processes, quantitative studies of the material injection from the surface into the plasma and the particle flow within the plasma must be performed.

In a companion study[14] we have determined the electron temperature in the surface-flashover anode plasma (5–8 eV) from observations of line-intensity ratios and time-dependent collisional radiative calculations.

In this study we present measurements of the time-dependent absolute intensities of line emission from various species and various charge states. Using two spectroscopic systems, two line intensities were observed in a single discharge reducing some ambiguities caused by shot-to-shot irreproducibilities. This was especially important for studying the relative abundances of different charge states of the same element. The observed line intensities were analyzed with the aid of a collisional-radiative code that yields the *time dependence* of the atomic level populations and of the ionization processes (for the time scale of 100 ns also the ionization rates depend on time). Using the observed electron temperature,[14] the measured time-dependent electron density in the plasma,[15] and time-dependent collisional radiative calculations we concluded that neutral particles, singly charged ions, and doubly charged ions are continuously injected from the anode surface into the plasma throughout the pulse. Although the time dependence of the material flux from the surface may be complicated, fluxes parabolic in time were used to fit the observed absolute line intensities. The satisfactory fits obtained for various elements and charge states gave the absolute time-dependent fluxes for the various species observed. The sensitivity of the determined particle fluxes to the plasma parameters was examined by repeating the analysis for three values of T_e within the uncertainty range of T_e. Furthermore, measurements and analysis of the particle injection rates into the plasma were also carried out for times after the main pulse, when the voltage on the diode was close to zero. The injection of neutral particles and some of the singly charged ions was found to continue after the pulse.

The findings show that singly and doubly charged ions are produced in the immediate vicinity of the dielectric surface. The higher the ionization rate is of an element on the surface with charge state z the fewer of this charge state and the more of charge state $(z+1)$ of that element are injected into the plasma. Using velocity distributions of various-charge-state ions, obtained from line Doppler broadening,[15] we inferred that the higher the charge state of the particles produced on the surface, the larger the kinetic energy with which they are injected. This suggests that the ions are accelerated into the plasma by electric fields on the anode surface, which is consistent with the observation[15] that the ions acquire their kinetic energy very close to the surface.

In order to compare particle fluxes from constituents of the dielectric anode and fluxes of particles also contained in surface adsorbates (the latter are mainly carbon, hydrogen, and oxygen) we admixed various compounds to the anode epoxy. We found that relative to their abundance in the dielectric, carbon and hydrogen were ejected with fluxes at least ten times larger than for elements admixed in the epoxy. The continuous particle injection into the plasma and the particle ionizations are shown to explain the observed rise in the areal electron density.

Using the determined particle fluxes and the observed particle velocity distributions[15] we calculated the ionization rates and the densities of ions and neutrals as they flow towards the outer region of the plasma. It is found that doubly charged ions and protons dominate the outer (ion-emitting) plasma region. This is consistent with charge-collector measurements on the extracted ion beam. Late in the pulse the ionization of hydrogen atoms traversing the plasma is shown to contribute a proton flux in the outer plasma region that is similar to the proton current density extracted into the diode acceleration gap. This proton flux due to hydrogen ionization may be important if the proton flow in the plasma penetrated by the magnetic field[16] is limited.

Both C III and proton fluxes are shown to rise with time in the outer plasma region. However, in this region, the C III to proton flux ratio rises from a low value to about half towards the end of the pulse. This rise is found to agree with the observed time-dependent C III to proton ratio in the extracted ion beam. The use of such investigations of the temporal and spatial dependences of the relative ionic densities in plasma source design is discussed.

The determination of the plasma composition allowed the electron energy losses due to inelastic collisions with the plasma particles to be obtained. These were found to be dominated by hydrogen ionization and impact excitations of C II and C III. As discussed in Ref. 14 these inelastic collisions are the main electron-cooling mechanism in the plasma.

II. EXPERIMENTAL ARRANGEMENT

The plasma investigated in these experiments is produced via a surface flashover of a dielectric sheet that serves as the anode in the planar magnetically insulated ion diode described in Ref. 15. The insulating magnetic field B_z in the diode was about 7 kG and the anode-cathode gap was 8 mm. The active anode was made of epoxy that filled grooves parallel to B_z in an aluminum plate. The height in the y direction of the active anode h_y was 6 cm and its length in the z direction l_z was 8 cm. The diode was powered by a 270-kV, 90-ns pulse delivered by an LC generator coupled to a 1-Ω water line. The diode voltage and current waveforms are given in Ref. 15.

The spectroscopic system is described in Ref. 14. In brief, light was collected along the z direction from the 3.5-cm-high central portion of the anode plasma ($l_y = 3.5$ cm). Most of the present measurements were integrated over the entire plasma thickness l_x [$l_x \simeq 2$ mm (Ref. 15)]. Using two spectrographs, intensities of two lines were measured in a single discharge with temporal and spectral resolutions of 5 ns and 0.1–0.5 Å, respectively. The simultaneous measurements of two line intensities, especially for lines of different charge states, helped to account for shot-to-shot variations that were usually less than 30%. The relatively high spectral resolution was

essential for examining the line shapes in order to reliably separate the observed lines from nearby impurity lines. The spectral range of the fiber array used at the spectrograph output was adjusted to obtain the entire profile of each line observed. Absolute calibration of each of the two spectroscopic systems over the entire spectrum (for each fiber channel) was performed using a few intensity-calibrated lamps. The estimated uncertainty in the absolute calibration is ±40%.

In order to observe the ejection of different particle species from the bulk of the dielectric anode, compounds of various elements were mixed with the epoxy used for the anode. We mixed powders of MgF_2, CaF_2, and $AlNaSiO_3$, each constituting 20% by weight of the entire mixture as in the previous studies.[14,15]

The self absorption along the line of sight was small for all presently observed lines (see Sec. III). Therefore, the intensity of line emission from a level u to a level l gives the population n_u of the upper level. The spatially averaged upper-level population was obtained from the total line intensity, expressed by the total current I_{ul} of the photomultiplier tubes that measure the light signal in the fiber array by

$$I_{ul}=n_u A_{ul} g_u l_x l_y l_z G R(\lambda) , \quad (1)$$

where A_{ul} is the Einstein coefficient, g_u is the degeneracy of the upper level ($g_u=2J+1$), G is the geometrical light collection efficiency, and $R(\lambda)$ is the system absolute calibration for the wavelength λ given in amperes per number of photons emitted per unit time from the plasma. Here, n_u is the absolute level population divided by the degeneracy as throughout the entire paper. The Einstein coefficients used for the determination of the upper-level populations will be given separately for each line observed.

III. MEASUREMENTS

It has been discussed in Ref. 15 that light from the plasma formed over the dielectric anode surface is first observed at $t\simeq 20$ ns after the start of the diode voltage pulse. At $t\simeq 50$ ns the plasma is seen to occupy an approximately 1.5-mm-wide region near the anode surface. Later on in the pulse the total amount of the plasma increases and the plasma appears to expand in the diode with a velocity of about 1 cm/μs. The line emission measurements reported here refer to the period subsequent to the plasma formation (i.e., for $t\gtrsim 20$ ns).

Examples of population densities are presented in Fig. 1 in which the populations of the C I($2p3s\ ^1P$), C II($3p\ ^2P_{3/2}$), and C III($2p^2\ ^1D$) levels, obtained from the intensities of the 2479-Å, 6578-Å, and 2297-Å lines, respectively, are given as a function of time. The hydrogen $n=3$ level population obtained from the H_α line intensity is presented in Fig. 2. In obtaining the absolute level populations the plasma thickness l_x [see Eq. (1)] was assumed to be 1 mm since line intensity axial distributions (as those given in Ref. 15) show that for each species most of the particles reside, throughout the pulse, in about a 1-mm-wide region in the plasma. Since C I, Mg I, Ca I, Al I, Mg II, and Ca II reside within $\simeq 0.5$ mm and H, C II, C III, and Al III within $\gtrsim 1$ mm from the anode surface, using $l_x=1$ mm gives densities lower than the actual densities in the plasma for the former group and higher for the latter one. The uncertainty in the absolute position-averaged level-population densities given in the

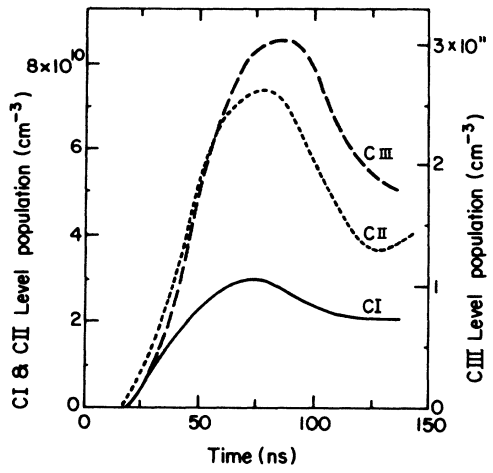

FIG. 1. Absolute level populations n_u (divided by the degeneracy) as a function of time after the start of the diode voltage pulse for C I ($2p3s\ ^1P$), C II ($3p\ ^2P_{3/2}$), and C III ($2p^2\ ^1D$) determined from the intensities of the 2479, 6578, and 2297 Å lines, respectively. Line emission was collected from the entire plasma. Two line intensities were measured in a single discharge allowing for normalization of intensities observed in different discharges. The uncertainties in the relative and in the absolute population densities are ±40% and ±70%, respectively. The latter is mainly due to the uncertainty in the absolute calibration and in the thickness $l_x=1$ mm assumed for the line-emitting plasma region.

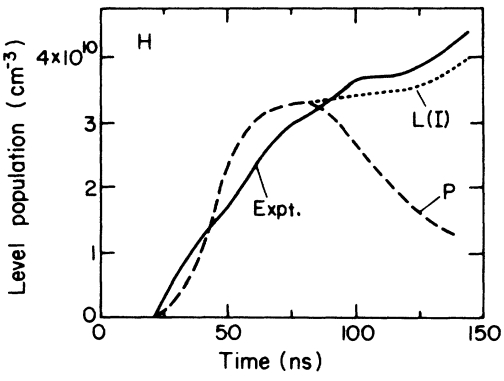

FIG. 2. Absolute population of the hydrogen $n=3$ level (divided by the degeneracy) observed from the H_α line intensity (solid line). The measurement uncertainty is as in Fig. 1. Also shown is the calculated population for the continuous P source of hydrogen in the ground state [curve P, see Eq. (3) and text in Sec. IV C] with $A(\mathrm{H})=2.5\times 10^{12}$ particles/cm^2 ns. The population for the L source (see Sec. IV D) is given by the curve L(I). For the calculations $T_e=7$ eV is assumed (Ref. 14). The measured electron density $\overline{n_e}(t)$ taken from Fig. 4(b) is used, as throughout the entire paper.

figures is ±70%, mainly resulting from the error in l_x for the various species and the uncertainty in the absolute calibration. The absolute material fluxes obtained below are not dependent on l_x since they give the particle number per unit area. The absolute and the relative uncertainties in the particle fluxes and the particle areal densities are estimated to be ±50% and ±30%, respectively, mainly due to the uncertainty in the relative calibration of the spectroscopic systems. A discussion of the effects of the uncertainties in the Einstein coefficients is given in Sec. IV G.

A general feature seen in Figs. 1 and 2 is that the line intensities start rising at $t \simeq 20$ ns and reach a near plateau at $t \simeq 70$ ns. For C II and C III the intensities drop between $t \simeq 95$ and 130 ns. Similar behavior has been seen for all the other H, C II, and C III line intensities observed.

Carbon and hydrogen species in the plasma can originate at adsorbates on our rough dielectric anode surface placed in an oil pumped diode environment. In order to study particle injection into the plasma from the dielectric material, we observed line intensities of particles contained in the epoxy mixture used for the anode. Thus, we measured line intensities of Mg I, Mg II, Ca I, and Ca II. Lines of Al I, Al II, and Al III were also observed. The origin of those particles is ambiguous since they may also originate from the aluminum ribs in the anode[15] as will be discussed in Sec. V C. For brevity we present time-dependent experimental and calculated level populations only for the magnesium species. The results for the other species will be summarized in the tables (see Sec. IV E). Figure 3 shows the observed level populations of Mg I and Mg II.

For each species we measured the intensities of several lines. This helped to compare several level populations to our code calculations for consistency checks and to rule out effects of impurity lines. Measuring intensities of two lines of a multiplet allowed us to verify the absence of impurity-line effects by confirming the scaling of the intensity with $(g_u A_{ul})$. The lines measured were the hydrogen H_α 6563 Å (upper level is $n=3$) and H_β 4861 Å ($n=4$); the C I 2479 Å ($2p3s\ ^1P$); the C II 6578 Å ($3p\ ^2P_{3/2}$), the 2512 Å ($2p^3\ ^2D_{5/2}$), 2509 Å ($2p^3\ ^2D_{3/2}$), 3921 Å ($4s\ ^2S_{1/2}$), and the 4267 Å ($4f\ ^2F$); the C III 2297 Å ($2p^2\ ^1D$); the Mg I 2852 Å ($3s3p\ ^1P$) and 3838 Å ($3s3d\ ^3D$); the Mg II 2796 Å ($3p\ ^2P_{3/2}$), 2798 Å ($3d\ ^2D$), and 2937 Å ($4s\ ^2S_{1/2}$), the Al I 3093 Å ($3s^23d\ D$) and 3082 Å ($3s^23d\ ^2D_{3/2}$); the Al II 2816 Å ($3s4s\ ^1S$); the Al III 3602 Å ($4p\ ^2P_{3/2}$), 5723 Å ($4p\ ^2P_{1/2}$), and 4529 Å ($4d\ ^2D$); the Ca I 4227 Å ($4s4p\ ^1P$); and the Ca II 3934 Å ($4p\ ^2P_{3/2}$) and 3968 Å ($4p\ ^2P_{1/2}$).

For carbon and hydrogen, line intensities have been measured for a pure epoxy anode as well as for epoxy anode with admixtures. The results were similar for both anodes indicating the absence of interference of lines of the admixed elements (Mg, Ca, Si, and Na) with the carbon and hydrogen lines. The interference of lines from adsorbates on the anode was examined by observing a few line intensities of H, O II, O III, N I, N II, and N III. This allowed us to estimate the intensities of strong lines of these species and to avoid observations of nearby lines.

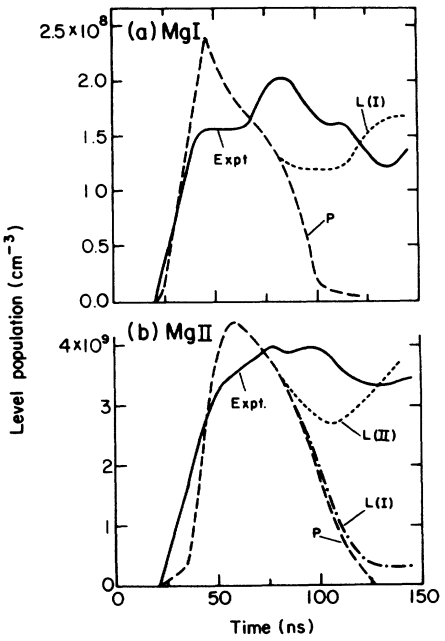

FIG. 3. Measured absolute populations (divided by the degeneracy) given by the solid lines. The measurement uncertainty is as in Fig. 1. (a) Mg I $3s3p\ ^1P$ level (obtained from the intensity of the 2852-Å line). The calculated population using the P source [Eq. (3), see Sec. IV C] with $A(\text{Mg I}) = 6.2 \times 10^7$ particles/cm^2 ns is given by the curve P. The population for the L source (see Sec. IV D) is given by the curve L(I). Here, $T_e = 7$ eV. (b) Mg II $3p\ ^2P_{3/2}$ level (2796-Å line). The calculated population using Mg I and Mg II P sources [Eq. (3), see Sec. IV C] is given by the curve P. The populations for an Mg I L source and an Mg II P source, and for both Mg I and Mg II L sources (see Sec. IV D), are given by the curves L(I) and L(II), respectively, Here, A(Mg I) is as in (a), $A(\text{Mg II}) = 7.8 \times 10^8$ particles/cm^2 ns, and $T_e = 7$ eV.

Similar precautions have been taken with respect to lines of the admixed elements. Note that an impurity line about 0.1 Å from the observed line could be resolved (see Sec. II).

We verified the absence of optical-thickness effects on our measurements. Using the upper-level populations obtained from Eq. (1) we estimated the corresponding lower-level populations with the aid of our collisional-radiative code. These lower-level populations, together with the measured[15] spectral line profiles, were used to estimate the line self absorption along the line of sight. Except for the C III 2297-Å line, the estimated self absorption for all observed lines was found to be small as confirmed by the experimental tests discussed in Ref. 15. The intensity of the 2297-Å line was corrected for the mild self absorption.

IV. DATA ANALYSIS

A. The time-dependence collisional-radiative code

The measured line intensities were analyzed with the aid of our collisional-radiative code that determines the level populations as a function of time by solving rate

equations of various atomic processes for given initial particle densities, see Ref. 14. A full description of the code is planned to be given in a future publication. Here, we shall give a general discussion and specify the rates used for the calculated atomic processes.

The code assumes experimentally determined electron density $n_e(t)$ and temperature $T_e(t)$ that are treated as input parameters. The use of the measured time-dependent electron density for the calculation of the level populations allowed us to ignore the change in the electron density due to the continuous particle ionization in our determination of the particle fluxes into the plasma. However, it is found *a posteriori* (see Sec. V B) that the measured rise in the electron density is consistent with the determined particle fluxes and ionizations in the plasma.

The description of our model for carbon is as follows. It consists of 7 levels for C I, 14 levels for C II, 42 levels for C III, and 10 levels for C IV. C I excitation rates are obtained from calculations given in Refs. 17 and 18. C II excitation rates for both spin-allowed and spin-forbidden transitions among the seven lowest levels are taken from the compilation of Itikawa *et al.*[19] Transition rates among higher levels are calculated using the analytical expression for the Gaunt factor given by Post and Jensen,[20] with the oscillator strengths given in Refs. 21–23. Ionization rates from the ground state and from higher levels of C I, C II, and C III are obtained using semiempirical fits to recent cross-section data, as is described in Ref. 24. Branching ratios into multiple final states for both ionization and recombination are also included by using the ratios of final-state degeneracies or, in the case of equivalent electrons, by using squared fractional parentage coefficients. C III excitation rates for both spin-allowed and spin-forbidden transitions among the 14 lowest levels are given in Ref. 19. Transition rates among higher levels in C III are calculated from the expressions given in Ref. 20, using oscillator strengths given in Refs. 21, 22, and 25. This modeling has been modified to include higher-n levels as discussed in Ref. 14.

Our magnesium model consists of the five lowest singlet levels for Mg I, 42 levels for Mg II ($n=3$ through $n=11$ levels), and the ground state for Mg III. The oscillator strengths for Mg I are taken from Ref. 26 which agrees with other calculations, as discussed in Ref. 27. The oscillator strengths for Mg II are taken from Lindgard and Nielsen[28] which agree to within 10% with Refs. 21 and 22.

The Al I model consists of 15 levels of Al I, and the ground state of Al II, Al II is not modeled in our code. The code for Al III includes 47 levels for Al III ($n=3$ through $n=12$) and the ground state of Al IV. It was verified that the addition of more levels did not alter the populations of the observed levels or the ionization rates. Oscillator strengths are taken from Refs. 21 and 22 for Al I and from Ref. 28 for Al III.

Calcium is modeled with 13 levels of Ca I, 19 levels of Ca II, and the ground state of Ca III. Oscillator strengths are taken from Refs. 21 and 22. Ionization and excitation rates for Mg I, Mg II, Al I, Al III, Ca I, and Ca II are taken from Ref. 20. Ionization and excitation rates for hydrogen are taken from Johnson's calculations[29] that were supported by measurements.[30]

The values of the electron density used were obtained from our Stark broadening measurements of the H_β line.[15] The measured electron density distributions $n_e(x,t)$ are shown for five times in Fig. 4(a). For simplicity, we use for the calculations a time-dependent position-averaged electron density $\overline{n_e}(t)$ that is shown in Fig. 4(b). The first time the electron density could be measured was $t=25$ ns. For the value of $\overline{n_e}(t)$ at $t_0=20$ ns, which is the earliest time at which line emission is detected (see Sec. III), we use the same value as for 25 ns. The uncertainty in the value of $\overline{n_e}(t)$, $\pm 20\%$, has little effect on the conclusions to be drawn here, as discussed in Sec. IV F.

The electron temperature T_e was determined in Ref. 14 to be between 5 and 8 eV. The temporal changes of T_e throughout the pulse were estimated to be within this uncertainty range. For simplicity we assume a constant value for T_e. We first analyze the line intensities assuming $T_e=7$ eV and then we discuss the sensitivity of our conclusions to changes in T_e between 5 and 9 eV (see Sec. IV F).

B. Instantaneous material source for the plasma

We now compare the observed temporal variation of the line intensities to predictions from our code by as-

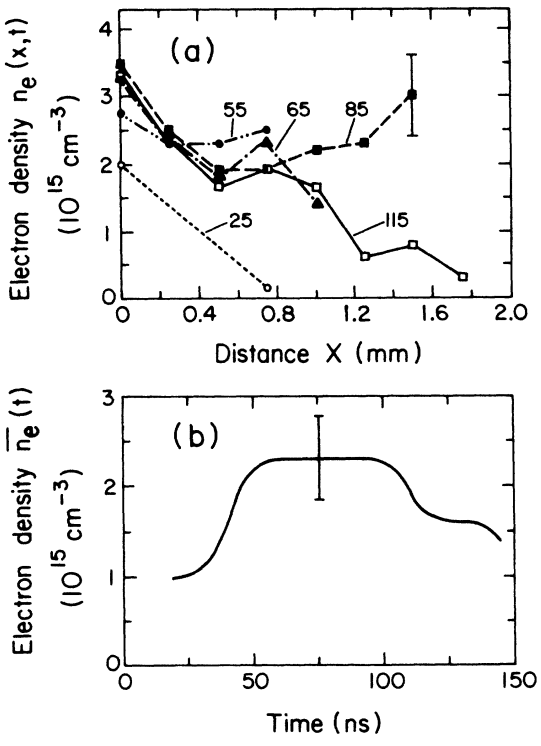

FIG. 4. (a) Electron density axial distribution $n_e(x,t)$ obtained from H_β Stark broadening, for five times (given in nanoseconds) throughout the pulse. The spatial resolution is $\simeq 0.3$ mm. The data points are connected by straight lines. (b) Electron density $\overline{n_e}(t)$ averaged over position as a function of time. The uncertainty in $n_e(x,t)$ and in $\overline{n_e}(t)$ is $\pm 20\%$ as indicated.

suming, in the first instance, that these variations result from time-dependent excitations and ionizations of material that is released from the anode surface early in the pulse. We assume for each species initial conditions of an instantaneous supply of particles into the anode plasma at $t=t_0$, i.e., the source function

$$S(i)=A(i)\delta(t_0)\ \text{particles/cm}^2\,\text{ns}\ , \qquad (2)$$

where $A(i)$ is the amplitude of species i and $\delta(t_0)$ is the δ function. At $t=t_0$ all species are assumed to be in the ground state. This assumption will be shown below to be of little importance for the present discussion.

Calculated populations of the C I $2p3s\ ^1P$ level and the C II $3p\ ^2P_{3/2}$ level are shown in Fig. 5(a) for an instantaneous C I source [Eq. (2)] assuming $T_e=5$ eV and using the measured electron density $\overline{n_e}(t)$ given in Fig. 4(b). The C II particles shown in this figure are produced from the ionization of C I. The C I excited-level population increases to a maximum in about 10 ns due to the fast equilibration time of the excited levels with the ground state of the same charge state. The population then decays in $\simeq 30$ ns due to ionization. This behavior is clearly inconsistent with the observed rise up to $t\simeq 70$ ns and the plateau of the C I level population shown in Fig. 1.

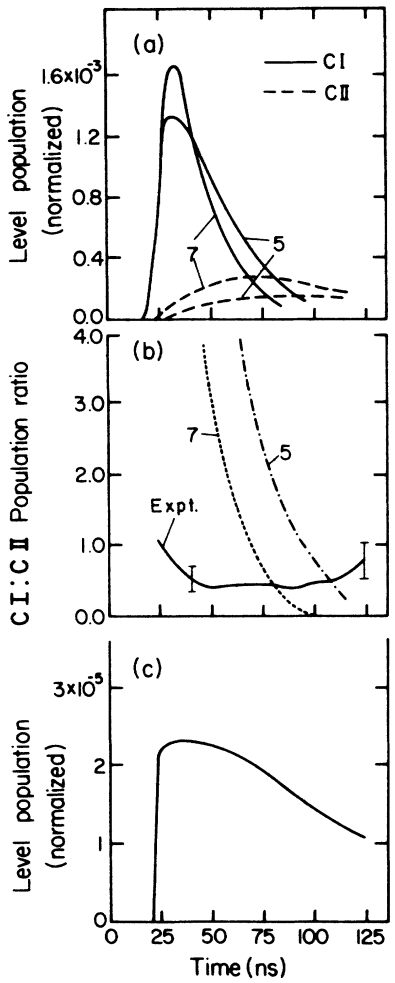

FIG. 5. (a) Calculated population of the C I $2p3s\ ^1P$ level for an instantaneous C I source [Eq. (2)], normalized to the total number of C I particles injected at $t=t_0$, as a function of time for $T_e=5$ and 7 eV (as indicated) using the measured $\overline{n_e}(t)$ given in Fig. 4(b). Also shown are the populations of the C II $3p\ ^2P_{3/2}$ level that result from C I ionization. (b) Calculated ratios of the C I $2p3s\ ^1P$ population to the C II $3p\ ^2P_{3/2}$ population for the same conditions as in (a) and for 5 and 7 eV as indicated. Also given is the experimental ratio (solid line) taken from the data in Fig. 1 with the indicated error bar of ±30%. (c) Calculated population of the hydrogen $n=3$ level, normalized to the total number of hydrogen atoms supplied instantaneously at $t=t_0$ [see Eq. (2)], for $T_e=5$ eV.

The discrepancy between the calculation and the observed level populations are even larger for higher electron temperatures within our uncertainty range. This is demonstrated in Fig. 5(a) which shows the faster C I ionization and level-population decay for $T_e=7$ eV. Furthermore, in the case of $T_e=7$ eV another discrepancy between the calculation and the observations is seen from the comparison of the calculated ratio between the C I and the C II level populations with the experimental ratio. These ratios are presented in Fig. 5(b). It is seen that for $t>75$ ns, due to the fast C I ionization into C II, the calculated ratio becomes much smaller than the experimental ratio. Since the C II amount cannot be reduced (it results from the C I ionization), the calculated ratio can increase only if an additional C I injection into the plasma is assumed to occur throughout the pulse.

Such calculations have been repeated for H, Mg I, Al I, and Ca I giving very similar conclusions both for the temporal variation of the level populations and for the ratio between the level populations of the neutral particles and of the singly charged ions. This is to be expected since the ionization times for these atoms are similar. For brevity, we present only the calculation for hydrogen [see Fig. 5(c)] showing, even for $T_e=5$ eV, the decay of the $n=3$ level population during the pulse, in disagreement with the measurement given in Fig. 2.

The main conclusion from the comparison is that an instantaneous supply of neutral particles [Eq. (2)] cannot explain the observed time dependence of the neutral-particle line intensities, namely the rise (up to $t\simeq 70$ ns) and the plateau. The conclusion is not sensitive to the values of $\overline{n_e}(t)$ within the uncertainty range of ±20%. This is because of the relatively short ($\lesssim 20$ ns) neutral-particle ionization time for this parameter range. Furthermore, if a large fraction of the particles delivered into the anode plasma at $t=t_0$ are excited rather than being at the ground state, as is assumed, the discrepancy between the calculations and the measurements would be even larger, since the C I ionization time would decrease.

C. Continuous material supply to the plasma

In order to explain the observed line intensities we suggest that particles are being continuously supplied from the anode surface into the plasma throughout the diode voltage pulse. In this study we do not attempt to understand the form of the ejection rate, thus, for the sake of simplicity, we suggest a source function parabolic in time common to all species observed. This parabolic function (called here the P source) is given by

$$S(i)=A(i)\left[\frac{(t-t_0)}{19}-\frac{(t-t_0)^2}{38^2}\right] \text{ particles/cm}^2\,\text{ns} . \quad (3)$$

It has its zeros at $t=t_0=20$ ns (the time at which the plasma is first observed, see Sec. III) and at $t=t_0+76=96$ ns as shown in Fig. 6(a). The value of $A(i)$, the peak ejection rate for species i, will be determined by fitting $S(i)$ to the measured line intensities. Using this source function, reasonably good fits for the observed line intensities during the pulse are obtained. More perfected fits can be obtained at the expense of complicating the source form, although this will have little effect on the inferred time-integrated amount of the material ejected (see Sec. IV E).

However, the P source will not explain all observed line intensities *after the main pulse* since for the neutral particles and certain singly charged ions ejection from the surface does not entirely stop at this time. For these species we shall use a source that allows continuing ejection for late times. This source (called here the L source) is obtained from the P source by keeping the value of the P source constant for $t>80$ ns, as shown in Fig. 6(a). The use of the L source for determining the ejection rates for some of the species after the pulse is postponed to Sec. IV D.

We now use the P source [Eq. (3)] to calculate the C I $2p3s\ ^1P$ level population for $T_e=7$ eV and $A(\text{C I})=9.4\times10^{10}$ particles/cm^2 ns. This is shown by the curve P in Fig. 6(b) together with the observed population taken from Fig. 1. It is seen that the continuous source function given in Eq. (3) gives a good agreement between the two populations for times up to $t\simeq80$ ns. For later times the calculated population is too low, indicating that unlike the P source, the actual C I source also continues at late times, as will be shown in Sec. IV D.

We now examine whether the C I continuous source may explain the observed C II level poulations. The calculated C II $3p\ ^2P_{3/2}$ level population resulting from ionization of C I is shown in Fig. 7(a). Also given are the calculated and the experimental ratios between the C II $3p\ ^2P_{3/2}$ and C I $2p3s\ ^1P$ level populations. The calculated C II level population is much smaller than the C I level population up to the end of the pulse (the ratio increases to 1 only at $t\simeq100$ ns), while the experimental ratio is about 2 throughout most of the pulse. This suggests the presence of an independent source for C II particles.

We would like to emphasize this result since it illustrates an important feature of the continuous source. The continuous source of C I at the ground state causes an increase in the excited level populations due to the fast excitations from the ground state and the relatively long C I ionization time. Also, because of the long ionization relaxation time,[1] the relative increase in the C I excited

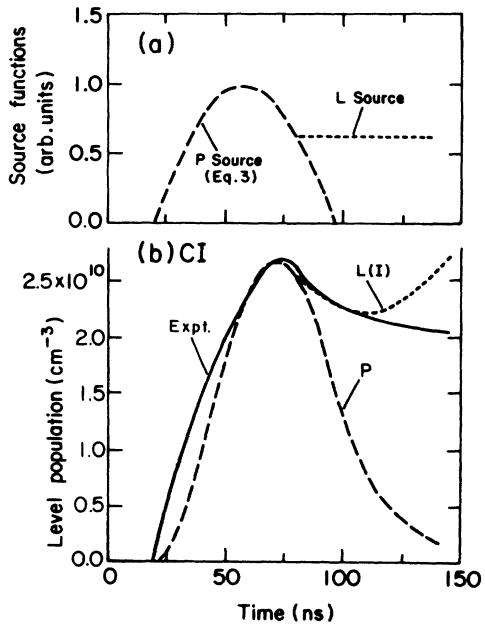

FIG. 6. (a) Illustration of the continuous parabolic source [P source, Eq. (3) with $A=1$] of particles in their ground state used for the calculations. The L source, used to describe the particle ejection after the pulse (see also Sec. IV D), is also shown. (b) The calculated C I $2p3s\ ^1P$ level population for a P source of C I in the ground state as given by Eq. (3) using $A(\text{C I})=9.4\times10^{10}$ particles/cm^2 ns (curve P), together with the measured population (solid line) taken from Fig. 1. Curve L(I) gives the calculated population using the L source, see Sec. IV D. Here, $T_e=7$ eV is assumed.

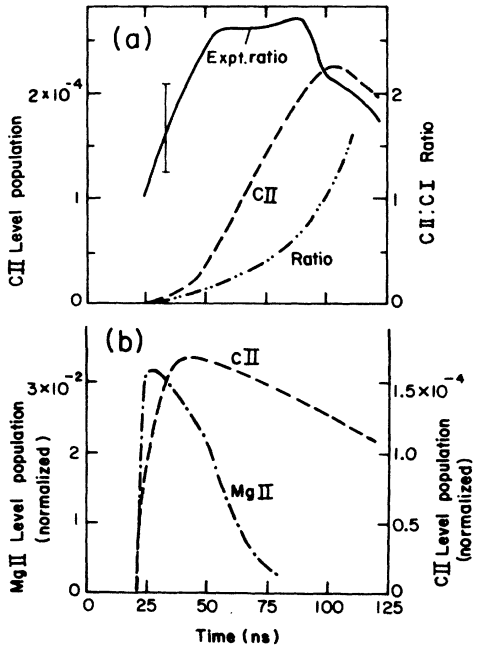

FIG. 7. (a) The calculated C II $3p\ ^2P_{3/2}$ level population for $T_e=7$ eV using a C I P source with $A=1$, together with the calculated ratio of the C II $3p\ ^2P_{3/2}$ population to the C I $2p3s\ ^1P$ population. Also given is the experimental ratio with the uncertainty of $\pm30\%$ as indicated. (b) The calculated C II $3p\ ^2P_{3/2}$ population for an instantaneous C II source [Eq. (2)], normalized to the total number of C II particles supplied at $t=t_0$, as a function of time. Also given is the calculated Mg II $3p\ ^2P_{3/2}$ population, for an instantaneous Mg II source, normalized to the total number of Mg II particles supplied at $t=t_0$. Here $T_e=5$ eV.

level populations due to the continuous C I injection is significantly larger than the relative increase in the C II density produced by the C I ionization. Therefore, while the C I source reproduces satisfactorily the experimental C I level population, it predicts too low populations for the C II levels. This point should be taken into account in inferring the densities of the higher charger states as will be discussed in Sec. V G.

As with C I, an instantaneous C II source at $t=t_0$ [as in Eq. (2)] is found to be inconsistent with the temporal variation of C II level populations. This is shown in Fig. 7(b), where it is seen that in the case of an instantaneous source at $t=t_0$ the C II level population, calculated for $T_e=5$ eV, reaches a maximum in about 20 ns and then decays throughout the pulse (due to the C II ionization). This is not consistent with the observed rising intensity presented in Fig. 1. A similar calculation for Mg II is also presented in Fig. 7(b) showing a large discrepancy between the calculated level-population decay and the experimental level population given in Fig. 3(b). The calculated level-population decay would be even faster for $T_e>5$ eV and thus even more inconsistent with the data. Thus, we suggest that also C II ions are continuously injected from the surface into the plasma. We assume the P source [Eq. (3)] with $A(\text{C II})=4.5\times10^{11}$ particles/cm^2 ns. The calculated C II level population, that results from both C I and C II P sources, is given by the curve P in Fig. 8(a) together with the data, showing a satisfactory agreement.

The C III $2p^2\,{}^1D$ absolute level population resulting from the ionization of C II (produced by the combined C I and C II P sources) is now calculated. This gives a population that is lower than the measurement given in Fig. 1. To match the calculated C III level population to the measurement we added an independent C III P source with $A(\text{C III})=2.3\times10^{11}$ particles/cm^2 ns. The resultant level population is presented by the curve P in Fig. 8(b) which shows a reasonably good fit to the data. Here we note that ionization of C III ions in the plasma can be neglected (the ionization time is greater than 10μs) and the $2p^2$ level-population decay at the end of the pulse is due to the decrease in the observed plasma density [see Fig. 4(b)].

Line intensities of all other neutral particles observed (H, Mg I, Al I, and Ca I) were satisfactorily explained by the continuous P source. Fits for H and Mg I are shown in Figs. 2 and 3(a), using the amplitudes $A(\text{H})=2.5\times10^{12}$ and $A(\text{Mg I})=6.2\times10^{7}$ particles/cm^2 ns. For hydrogen a good agreement between the calculated and the experimental level populations up to $t\simeq80$ ns is obtained (a better fit for $t>80$ ns will be discussed in Sec. IV D). The fit for Mg I for $t<80$ ns can be improved, if necessary, by modifying the source form as mentioned above.

The analysis of the line intensities of the singly charged ions Mg II and Ca II gives conclusions very similar to those for C II. For example, the Mg I P source [Eq. (3)] predicts an Mg II level population that is about ten times smaller than the experimental Mg II level population given in Fig. 3(b). Adding an instantaneous Mg II source at $t=t_0$ cannot explain the Mg II line intensity due to the fast decay of the calculated Mg II level population during the pulse as shown in Fig. 7(b). A continuous P source for Mg II is, therefore, suggested. The calculated Mg II level population due to the combined Mg I and Mg II P sources [using $A(\text{Mg II})=7.8\times10^{8}$ particles/cm^2 ns] is presented by the curve P in Fig. 3(b), showing a satisfactory fit up to $t\simeq80$ ns.

Since our code does not include as yet a satisfactory modeling for Al II ions, we could not obtain the Al II ejection rate. For Al III we use a P source that is meant to represent the combined Al III supply due to Al II ionization and due to direct Al III flux from the surface. Such a source, using $A(\text{Al III})=1.9\times10^{10}$ particles/cm^2 ns, provides a good fit to the measured Al III line intensity.

In our model of the continuous particle source we neglected the material density at $t=t_0$. This is justified *a posteriori* since the level populations throughout the pulse

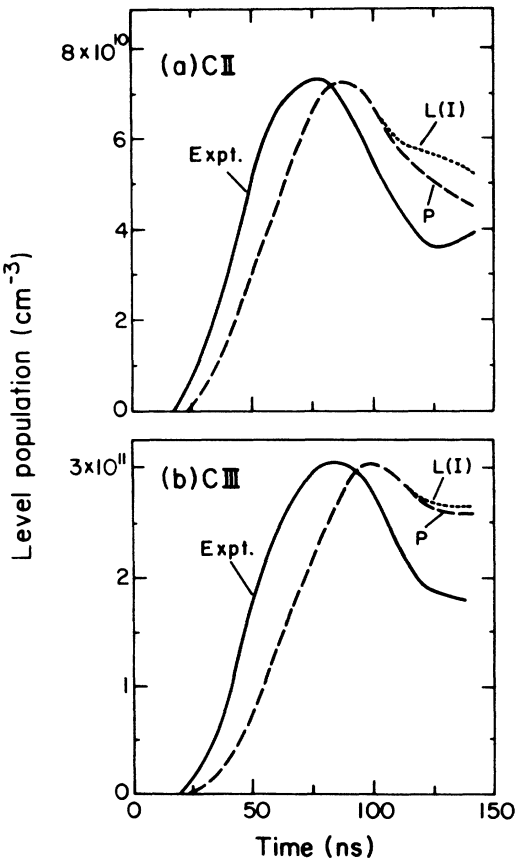

FIG. 8. (a) The calculated C II $3p\,{}^2P_{3/2}$ population for P sources of C I and C II in their ground states [Eq. (3)] using $A(\text{C I})=9.4\times10^{10}$ and $A(\text{C II})=4.5\times10^{11}$ particles/cm^2 ns (curve P), together with the observed level population taken from Fig. 1 (solid line). Here $T_e=7$ eV [as in Fig. 6(b)]. Also shown are the calculated populations for a C I L source and a C II P source [curve L(1), see Sec. IV D]. (b) Calculated population (curve P) of the C III $2p^2\,{}^1D$ level for P sources of C I, C II, and C III using A(C I) and A(C II) as in (a) and $A(\text{C III})=2.3\times10^{11}$ particles/cm^2 ns, together with data from Fig. 1 (solid line). Also shown is a calculation using the L source for C I and the P sources for C II and C III [curve L(1), see Sec. IV D]. Here $T_e=7$ eV.

were shown to be dominated by the particle supply at $t > t_0$. Also, we assumed that the particles supplied are in the ground state. The possibility that the injected particles are excited due to electron-impact excitations close to the anode surface (in keeping with the discussion in Sec. V A) would have little effect on our fitted level populations.

In determining the actual ionic source amplitudes the ion losses to the diode acceleration gap should also be considered. The proton losses to the diode gap are unimportant for this discussion since the determination of the neutral hydrogen source is not affected by the proton density (recombination is negligible). The losses of the other singly charged ions are believed to be small since these ions are shown not to reach the outer (ion-emitting) region of the plasma (see Sec. V D). Most of the extracted nonprotonic ions are doubly charged ions, where the C III ions are dominant due to their largest abundance in the plasma and their relatively fast motion towards the outer plasma region (see Sec. V D). Thus, we assume that all nonprotonic ions in the beam, found from charge-collectors measurements to constitute about 50% of the ion current (see Sec. V E), are C III ions. The total ion current density was observed to rise during the pulse to about 100 A/cm^2. We thus infer that the total time-integrated C III losses to the diode acceleration gap during the pulse is 8×10^{12} particles/cm^2. Accounting for the C III losses to the gap increases the amount of the C III ejection rate from the anode surface from the value $A(\text{C III})=2.3\times10^{11}$ used in Fig. 8(b) to 3.8×10^{11} particles/cm^2 ns. This value for A(C III) is the one given in Table I (see Sec. IV E), since it represents the actual source amplitude for C III.

D. Material ejection after the pulse

As already indicated the release of neutral particles from the anode surface does not drop to zero as the P source [Eq. (3)] does. Indeed, using the L source [see Fig. 6(a) and text in Sec. IV C], which allows continuing ejection late in the pulse, gives a better fit for the neutral-particle line intensities for this period of time. The neutral-particle level populations calculated with the L source are shown by the curves $L(I)$ in Figs. 2, 6(b), and 3(a) for H, C I, and Mg I, respectively. Clearly, the L source fits the observed populations after the pulse better than the P source for all the neutral particles observed.

The use of the L source for the ions, however, is not always justified. Let us first look at the C II level popula-

TABLE I. Measured peak (at $t\simeq80$ ns) level populations n_u per cubic centimeter for C I, C II, C III, and hydrogen. Also given are the calculated total particle densities n_t, inferred from n_u, the amplitudes of the source functions $A(i)$ [see Eq. (3)], and the total number N of particles supplied directly from the surface into the anode plasma (not including the particles produced by ionization of the lower charge states) up to $t=t_0+76=96$ ns. In obtaining N for C I and H we used the L source (see Sec. IV D). The fraction of ions at $t=96$ ns that results from the ionization in the plasma of the lower charge states is given by f. For A, N, and f for C III, the C III losses to the diode acceleration gap have been taken into account (see Sec. IV C). Also given is the ionic charge density Q and the total charge density Q_t due to C II, C III, and protons produced by hydrogen ionization in the plasma (not including direct proton ejection from the surface). In obtaining the average particle and charge densities the plasma thickness l_x [see Eq. (1)] was assumed to be 0.1 cm. The results are given for $T_e=7$, 5, and 9 eV (for 5 and 9 eV see Sec. IV F). The measured time-dependent electron density used for the calculations is given in Fig. 4(b). The numbers in square brackets are powers of 10.

Atomic level	T_e (eV)	n_u (cm^{-3}) (±70%)	n_t (cm^{-3}) (±70%)	A (cm^{-2} ns^{-1}) (±50%)	N (cm^{-2}) (±50%)	f (±40%)	Q (e/cm^3) (±70%)
C I $2p3s\ ^1P$	7	2.5[10]	1.1[13]	9.4[10]	5.2[12]		
C II $3p\ ^2P_{3/2}$	7	6.6[10]	2.2[14]	4.5[11]	2.3[13]	0.16	2.2[14]
C III $2p^2\ ^1D$	7	2.8[11]	1.2[14]	3.8[11]	2.0[13]	0.25	2.4[14]
$H(n=3)$	7	2.8[10]	6.6[14]	2.5[12]	1.4[14]		
Protons	7		3.9[14]				3.9[14]
Q_t							8.5[14]
C I $2p3s\ ^1P$	5	2.5[10]	1.3[13]	7.1[10]	4.0[12]		
	9		9.6[12]	1.2[11]	6.8[12]		
C II $3p\ ^2P_{3/2}$	5	6.6[10]	3.9[14]	8.3[11]	4.2[13]	0.06	3.9[14]
	9		1.6[14]	3.3[11]	1.7[14]	0.27	1.6[14]
C III $2p^2\ ^1D$	5	2.8[11]	2.6[14]	7.2[11]	3.6[13]	0.07	5.2[14]
	9		8.1[13]	2.5[11]	1.3[13]	0.52	1.6[14]
$H(n=3)$	5	2.8[10]	1.3[15]	3.5[12]	2.0[14]		
	9		4.5[14]	2.3[12]	1.3[14]		
Protons	5		2.9[14]				2.9[14]
	9		4.7[14]				4.7[14]
Q_t	5						12[14]
	9						7.9[14]

tion shown in Fig. 8(a). The calculated population for a C I L source and a C II P source [curve $L(I)$] is somewhat larger than the measured C II population. Assuming a direct ejection of C II also after the P source results in an even larger deviation from the measurement. This conclusion is not dependent on the electron temperature assumed as can be seen from the fits given in Fig. 9 for $T_e=5$ eV (see Sec. IV F). Contrary to this, the calculated line intensities for Mg II [see Fig. 3(b)], using P sources for the neutral particles and the singly charged ions, are too small for $t>80$ ns [see the curve P in Fig. 3(b)]. Using an L source for the neutral particles increases the level populations of the singly charged ions very little, as shown by the curves $L(I)$ in Fig. 3(b). L sources for both the neutral particles and the singly charged ions are required to reproduce the observed intensities for this period of time as shown by the curves $L(II)$ in Fig. 3(b). Similarly, it is found that an L source is required also for Ca II. A plausible explanation for the absence of the C II ejection and the continuing ejection of Mg II and Ca II for $t>80$ ns is discussed in Sec. V A.

For the doubly charged ions C III and Al III P sources [Eq. (3)] provide reasonable fits for the measured populations, see Fig. 8(b) for C III. Continued ejection near the end of the pulse for doubly charged ions predict many more of these ions than found experimentally. We also note that the use of the L source for the neutral particles leaves the level populations of the doubly charged ions practically unchanged. This is shown in Fig. 8(b) for C III, where the C III level population calculated using an L source for C I is given by the curve $L(I)$.

E. Particle fluxes and densities

In Tables I and II we summarize some of the quantities obtained in our analysis for the various species. We present the absolute level populations n_u observed during the plateau period ($t\simeq 70$–95 ns) together with the total particle density n_t calculated using n_u. We also give the amplitude A of the best-fit P source [Eq. (3)] and the total amount N injected per square centimeter into the plasma up to the end of the source at $t=t_0+76=96$ ns. For the total number N of the neutral particles, Mg II, and Ca II supplied up to $t=96$ ns, we use the L source [see Fig. 6(a)] which gives an N larger by 10% than the P source. Here, N for each species refers only to the direct ejection from the surface. We note here that improving the fitting of the sources by using source forms other than the parabolic form is estimated to change N by approximately 10%. The total number of ions per square centimeter present in the plasma at the end of the pulse, including the fraction contributed by ionization of the lower charge states, can be obtained by multiplying n_t given in the tables by 0.1 cm which is the plasma thickness used in Eq. (1). The ion fraction f that results from ionization of the lower charge states is also given. In Table I we also give the charge density Q of carbon ions and of protons produced by hydrogen ionization (direct proton injection is not included since it has not been determined in this study, see further in Sec. V B) as well as the resulting total charge density Q_t. The calculated Q and the results for $T_e=5$ and 9 eV given in Table I are discussed in Sec. IV F.

Note that the density ratios of the different charge states in our plasma, being determined by ionization and time-dependent particle fluxes into the plasma (recombination is very slow), are very different from the steady-state ratios. For example, the calculated steady-state density ratios of C I:C II:C III, using $n_e=2.3\times10^{15}$ and $T_e=7$ eV, are $1:2\times10^5:2\times10^7$, while these ratios for our plasma are 1:20:11 (see Table I). This emphasizes the need for time-dependent measurements and calculations for determining the plasma composition in experiments in which 100-ns-duration plasmas are considered.

F. Sensitivity of the analysis to the plasma parameters

We now discuss the sensitivity of the determination of the source functions to the values of n_e and T_e. Varying n_e and T_e within the uncertainty ranges (±20% and 5–8 eV, respectively) does not alter the conclusions drawn above, namely, the need for continuous particle sources. What does change in the fits with varying n_e and T_e are the absolute source amplitudes. We will discuss the changes in the source amplitudes only for hydrogen and carbon species which are the major plasma components. The uncertainty in $\overline{n_e}(t)$ causes an uncertainty of ±20% in the inferred source amplitudes. The uncertainty in T_e has a larger effect. In Fig. 9 we give the calculated level populations for the best-fit P sources [Eq. (3)] for C I, C II, and C III using $T_e=5$ eV. The amplitudes used are

TABLE II. Measured and calculated results, as in Table I, for Mg I, Mg II, Al I, Al III, Ca I, and Ca II. In the calculations $T_e=7$ eV. In obtaining N for Mg I, Mg II, Al II, Ca I, and Ca II, the L sources were used (see Sec. IV D). The numbers in square brackets are powers of 10.

Atomic level	n_u (cm^{-3}) (±70%)	n_t (cm^{-3}) (±70%)	A ($cm^{-2}ns^{-1}$) (±50%)	N (cm^{-2}) (±50%)	f (±40%)	Q (e/cm^3) (±70%)
Mg I $3s3p\ ^1P$	2.0[8]	3.5[9]	6.2[7]	3.5[9]		
Mg II $3p\ ^2P_{3/2}$	3.9[9]	8.6[10]	7.8[8]	4.3[10]	0.08	8.6[10]
Al I $3s^23d\ ^2D_{5/2}$	2.6[8]	1.3[11]	3.5[9]	2.0[11]		
Al III $4p\ ^2P_{3/2}$	7.0[9]	5.9[12]	1.9[10]	9.6[11]		1.2[13]
Ca I $4s4p\ ^1P$	1.8[8]	1.7[9]	5.8[7]	3.3[9]		
Ca II $4p\ ^2P_{3/2}$	2.2[9]	6.2[10]	3.5[8]	2[10]	0.20	6.2[10]

$A(\text{C I})=7.1\times10^{10}$, $A(\text{C II})=8.3\times10^{11}$, and $A(\text{C III})=5.6\times10^{11}$ particles/cm^2 ns giving satisfactory fits. The main difference between the fits for 5 and 7 eV is that for 5 eV the P source for C I predicts a level population for $t>80$ ns closer to the experiment than the P source for 7 eV. This results from slower C I ionization for $T_e=5$ eV. However, also for $T_e=5$ eV an L source for C I is required to explain the level population after the pulse, as shown by the curve $L(\text{I})$ in Fig. 9(a). The fits for hydrogen for 5 eV for both a P source and an L source are shown in Fig. 10, leading to the same conclusions. Such fits were also repeated for $T_e=9$ eV giving similar results.

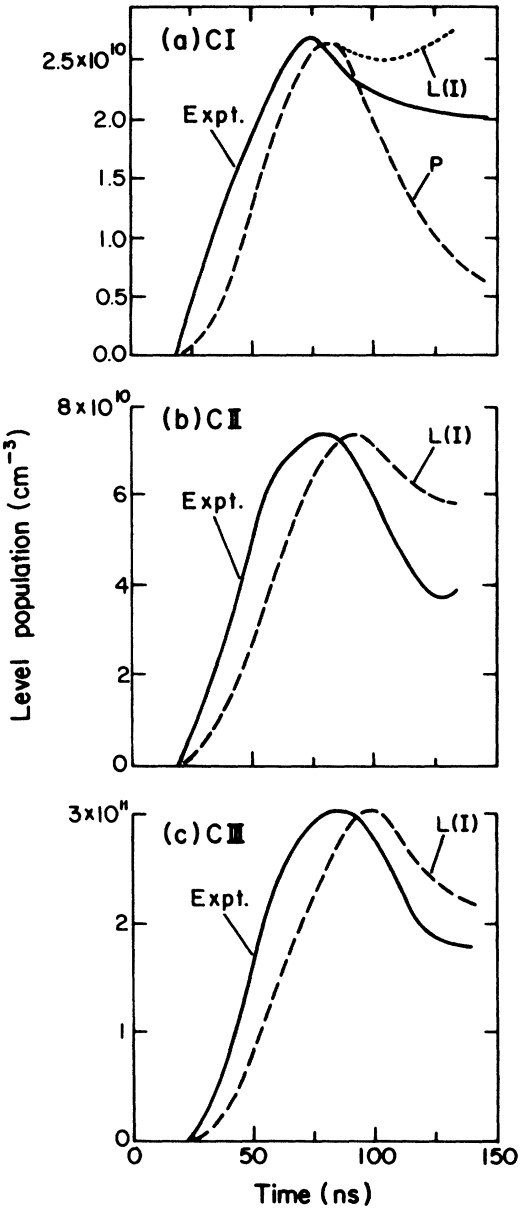

FIG. 9. Calculated level populations for C I, C II, and C III for $T_e=5$ eV, together with the data taken from Fig. 1 (solid lines). (a) The C I $2p3s\ ^1P$ level using $A(\text{C I})=7.1\times10^{10}$ particles/cm^2 ns. The curves P and $L(\text{I})$ correspond to a P source [Eq. (3)] and an L source, respectively. (b) The C II $3p\ ^2P_{3/2}$ level using the C I L source as in (a) and a C II P source with $A(\text{C II})=8.3\times10^{11}$ particles/cm^2 ns [curve $L(\text{I})$]. (c) The C III $2p^2\ ^1D$ level using the C I L source, the C II P source, and a C III P source with $A(\text{C III})=5.6\times10^{11}$ particles/cm^2 ns [curve $L(\text{I})$].

In Table I we summarize the calculated results obtained from the best-fit sources for 5 and 9 eV. It is seen that the inferred source amplitudes depend on the T_e assumed. For the uncertainty range of our T_e, 5–8 eV,[14] $A(\text{C I})$, $A(\text{C II})$, and $A(\text{C III})$ vary by factors smaller than 2, 3, and 3, respectively. The hydrogen ejection rate varies by 50%. Also the fraction of ions f produced by ionizations of the lower charge states and the relative abundance of carbon ions and protons (produced only by hydrogen ionization in the plasma) are dependent on T_e. Similar uncertainties, due to the uncertainty in T_e, have to be assumed for all other species reported. It is seen in Table I that the calculated total charge density Q_t varies by only ±20% within the temperature range of 5–8 eV. In Sec. V B the total charge density is used to obtain the rise in the total plasma areal density during the pulse.

G. Comparison of the calculations with further observations

We note here an additional experimental consistency with our calculations. Experimental verification of the plasma optical thickness for a line transition gives an estimate for the population of the lower level. While this was helpful for examining our estimates of atomic level populations it was especially important for estimating the ground-state population (when a transition to the ground state could be observed). We used this method to estimate the ground-state population of Mg II. As discussed in Ref. 15, the spectral width of the Mg II 2796 Å ($3p\ ^2P_{3/2}\rightarrow3s\ ^2S_{1/2}$) line was found to vary within about 10% with the active anode length up to $l_z=14$ cm. Since a 10% increase in the width corresponds to an optical thickness τ of about 0.5 this gives approximately 1.2×10^{11} cm^{-3} for the population difference between the ground state and the first excited state. Calculations

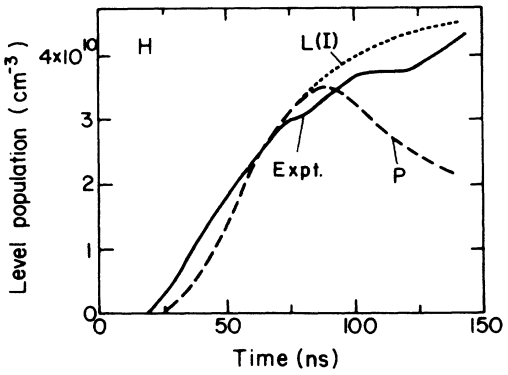

FIG. 10. The calculated H $n=3$ level population using the P source [Eq. (3)] with $A(H)=3.5\times10^{12}$ particles/cm^2 ns (curve P) and the L source [curve $L(\text{I})$], together with the experimental data from Fig. 2 (solid line). Here $T_e=5$ eV.

based on our experimental line intensities give for Mg II during the plateau period a population difference that agrees with the estimate established here. (Remember that populations are always divided by the degeneracy factor.)

In our analysis we have not discussed the calculations for all line intensities observed for each species. Almost all calculated line intensities were consistent with the measured intensities discussed above except for the ratio between the C III $2p^2$ level population and the populations of the higher C III levels as discussed in Ref. 14. However, in order to obtain the C III ground-state density we used our code and the absolute population of the $2p^2$ level, the lowest level observed, as discussed in Sec. IV C and IV D. This gave a reasonable C III density (see Table I), while the observed C III high-level populations together with the code calculations give five times higher densities. The use of the $2p^2$ level population to obtain the C III ground state density is justified on the basis of line-intensity ratio measurements made in the edge plasma of the TEXT tokamak.[31] In these measurements the intensity ratio of the $2s2p\ ^3P$–$2p^2\ ^3P$ transition to the $2s^2\ ^1S$–$2s2p\ ^1P$ transition was found to be in good agreement (to within the experimental uncertainty of approximately 20%) with calculations from a C III model that uses collisional excitation and deexcitation rates based on R-matrix calculations of Berrington.[32] In these studies[31] independent temperature and density measurements of the edge plasma were used to allow a direct comparison of measurements with predictions from the code. Similar experimental agreement was found for the intensity ratios for other Be-like ions (O V, F VI, Ne VII). This good agreement for transitions amongst the $n=2$ levels is attributed to the accuracy of the R-matrix calculations which include resonance effects.

In order to estimate the sensitivity of the inferred particle fluxes to uncertainties in process rates used in the code, we recalculated C III fluxes using either different radiative decay rates or different excitation rates. Decreasing all radiative decay rates A_{ik} by 30% (and not changing the excitation and deexcitation rates), which is a reasonable estimate for their average uncertainty, resulted in an increase in the C III flux by approximately 10%. Decreasing excitation and deexcitation rates by 30% (and not changing A_{ik}) resulted in a 30% decrease in the C III flux. Measurements of spectral intensities from Be-like ions in θ-pinch plasmas[33,34] have suggested that a few particle excitation and radiative decay rates may be incorrectly calculated by as much as a factor of 2. However, we have found that the $2p^2\ ^1D$ population, as calculated in the code, is insensitive to changes in these particular transition rates, and thus would cause little additional uncertainty in the magnitude of the C III flux. Finally, we also recalculated the Mg I and Mg II fluxes using oscillator strengths smaller by 30%, which also reduced the rates of the radiative decays, excitations, and deexcitations. This increased the inferred Mg I and Mg II fluxes by less than 15%. All changes in the rates were found to have no significant effect on the general shape of the population time history. Thus, only the magnitudes of the particle fluxes are found to be sensitive to changes in the rates, and therefore our conclusions on the occurrence of a continuous supply of material are unaffected by these uncertainties.

Optical thickness effects in the calculations were examined as described in Ref. 14. Mild thickness was found only for the C II $2s2p^2\ ^2P \rightarrow 2s^2 2p^2\ ^2P$ transition and the C III $2s2p\ ^1P \rightarrow 2s^2\ ^1S$ transition. Accounting for this optical thickness increased the populations of a few levels only slightly relative to the case of optical thinness and did not affect the ionization rates or the inferred C III total density.

V. DISCUSSION

A. Particle fluxes into the plasma

The temporal variations of the absolute line intensities of neutrals and ions of various elements were clearly shown to be inconsistent with the assumption that all the material from which the plasma is produced is ejected from the anode surface only early in the pulse. This assumption also led to large inconsistencies with the observed ratios between the intensities of the neutral-particle lines and the singly charged ion lines of the same element. On the other hand all the observations were satisfactorily explained by assuming a continuous flow of material into the anode plasma (evidently from the anode surface). Material flux of a simple form, parabolic in time, was found to give reasonably good fits for several neutral particles and ions observed in the plasma. Material ejection after the diode voltage pulse was also found. The processes responsible for the release of material into the anode plasma during and after the voltage pulse are not known and a considerable experimental effort is required for their understanding. In Ref. 15 we reported that neutral particles and ions are injected into the plasma with kinetic energies of about 8 and 20–80 eV, respectively. The mechanism responsible for production of such high energies is also as yet not understood. Also, the factors that determine the temporal shape of the material flux are not known.

Our model suggests that singly and doubly charged ions are continuously injected into the plasma. Such ions could possibly be produced very close to the anode surface by electron-impact ionization of neutral particles released from the surface. The electron temperature and density near the surface are not known. Assuming there is an electron temperature similar to that observed in the plasma (7 eV) we calculate the time-dependent ionization rates of C I and C II a few nanoseconds after being ejected from the surface. It is found that electron densities of about 10^{17} cm^{-3} would be required to produce enough singly charged and doubly charged carbon ions in about 2 ns. During such a period the ejected particles probably reside within 10 μm near the anode surface as found in studies of insulator electrical breakdown.[35] Such electron densities are not unreasonable taking into account that particle densities approximately greater than 10^{17} cm^{-3} are believed[35] to exist within a few microns from dielectric surfaces undergoing flashover.

Following the suggestion of ion production in the immediate vicinity of the anode surface, one expects that for

neutral particles which have higher ionization rates, a larger fraction would be ionized into singly charged ions. The actual injection rate of the singly charged ions would also be dependent on their ionization on the surface into doubly charged ions. However, it is likely that the higher the ionization rate of a neutral particle, the larger would be the ratio of the singly charged ion ejection rate to that of the neutral particles. Neutral ionization rates on the anode surface are not known. However, in the anode plasma we calculate ionization times of 3–5 ns for Mg I and Ca I, while C I ionizes in approximately 20 ns. Mg I and Ca I are expected to ionize faster than C I also on the surface. Therefore, it is not surprising that the source-amplitude ratios $A(\text{Mg II})/A(\text{Mg I})$ and $A(\text{Ca II})/A(\text{Ca I})$ are found to be 12 and 6, respectively, larger than $A(\text{C II})/A(\text{C I})\simeq 5$ (see Tables I and II for 7 eV). Note that $A(\text{C III})/A(\text{C II})$ is $\simeq 0.8$ (see Table I for 7 eV), smaller than $A(\text{C II})/A(\text{C I})$. This may result from the relatively long C II ionization time (for comparison, the C II ionization time in the plasma is $\simeq 100$ ns).

The ejection of neutral particles from the surface and the ejection of Mg II and Ca II were clearly observed to continue after the end of the diode voltage pulse (see Sec. IV D). On the other hand, the ejection of C II, C III, and Al III were observed to be consistent with a parabolic drop to zero (the P source) at the end of the pulse ($t\simeq 95$ ns). This finding can also be explained by considering the particle ionization close to the surface. It is plausible that the ionization rates for all particles decrease for no applied electric field. Thus, neutral particles and singly charged ions of fast ionizing neutral atoms (Mg II and Ca II) would still be formed on the dielectric surface and thus injected into the plasma. The injection of C II ions and doubly charged ions (due to the slower ionization of C I and of the singly charged ions on the anode surface) would drop considerably.

We now suggest the possibility that the ions acquire a large portion of their kinetic energies observed in the anode plasma[15] close to the anode surface, presumably due to electric fields on the surface. This is consistent with the fact that the particle energies have been observed to be large over the entire plasma to within approximately 100 μm from the surface.[15] A possible reason for the neutral-particle kinetic energies may be charge-exchange collisions of the accelerating ions. Ions produced on the surface must be assumed to acquire energies higher than the neutral particles in order to explain the higher kinetic energies observed for the ions in the plasma. Ions produced in the plasma due to the ionization of neutral particles injected into the plasma would retain the neutral-particle kinetic energy. Therefore, for a small f (see Table I), i.e., for a large fraction of the singly charged ions that stream directly from the surface, one should expect a larger velocity in the plasma of the singly charged ions relative to that of the neutral particles. Indeed, the kinetic energy of Mg II (with $f=0.08$, see Table II), averaged over the main diode pulse ($t<100$ ns), was found to be approximately equal to 27 eV as compared to 9 eV for Mg I.[15] Similarly, C II ions with $f=0.16$ (see Table I for 7 eV) were found to have an energy of approximately 18 eV as compared to the C I energy of 7 eV.

Singly charged ions with higher ionization rates would more easily ionize into doubly charged ions close to the anode surface. The details of the ion acceleration near the anode surface are not known. However, ion acceleration close to the surface is consistent with doubly charged ions streaming with kinetic energies higher than those of the singly charged ions. Indeed, part of the C III ions are injected directly from the surface (rather than being produced by C II ionization in the plasma, see Table I) and the average C III kinetic energy was found to be about 20% larger than the C II energy.

Additional support for this relation between the ionizations near the surface and the particle kinetic energies in the plasma comes from the observed silicon ion energies. The Si II ions ionize much faster than C II. Thus, we expect a significant production of Si III on the anode surface. The Si III ions in the plasma are, therefore, expected to originate mainly at the anode surface and to stream into the plasma with kinetic energies lager than the Si II ions. Indeed, the Si III energy in the plasma during the pulse was found to be 40–80 eV while the Si II energy was 20–30 eV. This is consistent with our suggestion that, due to electric fields on the anode surface, the doubly charged ions produced on the surface acquire more kinetic energy than the singly charged ions. The Si IV ions in the plasma, due to the slower ionization of Si III on the anode surface, are very likely to result from the ionization of Si III in the plasma. This is consistent with the similar kinetic energies observed for Si III and Si IV.[15]

B. Plasma density

The use of the measured average plasma electron density $\overline{n_e}(t)$ in our calculations allowed us to model the material supply to the plasma on the basis of the known instantaneous electron density and avoid the need to calculate the charge in the electron density due to ionization. We can now use our determined particle fluxes and our calculated ionic densities to obtain the time history of the total number of electrons in the plasma. Comparing this to the experimental electron density will provide a test of our model and will also be useful in quantifying the contribution of the various fluxes to the plasma density.

Since the plasma ions are mainly protons and carbon ions we restrict our discussion to these particles. Thus, the total electron number $N_e(t)$ per cm^2 in the plasma is given as a function of time by

$$N_e(t)=N_e(t_0)+N(\text{C II},t)+2N(\text{C III},t)+N(p,t)-\int_{t_0}^{t}\frac{J_i}{e}dt\ , \tag{4}$$

where $N_e(t_0)$ is the total electron number at t_0, at which time the plasma is first observed. Here, $N(\text{C II},t)$, $N(\text{C III},t)$, and $N(p,t)$ are the total time-dependent numbers of C II, C III, and protons produced in the plasma as a result of the continuous particle supply (after t_0). The last term in Eq. (4) accounts for the ion losses to the diode acceleration gap (e being the electron charge). It was obtained from charge-collector measurements (see

Sec. V E here and Ref. 14) which showed that the ion current density J_i rises during the pulse to approximately less than 100 A/cm^2 and it modifies $N_e(t)$ by about 10%.

Our code calculations of $N(\mathrm{C\,II},t)$, $N(\mathrm{C\,III},t)$, and $N(p,t)$ are given in Fig. 11(a) for $T_e=7$ eV. In calculating $N(p,t)$ only the protons produced by the hydrogen ionization are counted, since the direct proton injection has not been determined. Using Eq. (4) we can now obtain the total electron number in the plasma $N_e(t)$ and compare it with the experimental number

$$N_e^{\mathrm{expt}}(t)=\int_0^{x_m} n_e(x,t)dx \ ,$$

obtained from integration of the measured electron density distribution. Here, x_m is the farthest position for which the H_β line was intense enough to allow the line profile to be obtained with a reasonable accuracy. Examples of such distributions are given in Fig. 4(a) and in Ref. 15. In Fig. 11(b) we present $N_e(t)$ curves calculated for the temperatures 5 and 7 eV, showing that the rise of $N_e(t)$ is similar to that of $N_e^{\mathrm{expt}}(t)$. The calculated $N_e(t)$ appears to be smaller than $N_e^{\mathrm{expt}}(t)$. This is to be expected since in these calculations we did not include the direct proton ejection from the anode surface. Direct proton ejection probably occurs since direct ejections were observed for all singly charged ions studied.

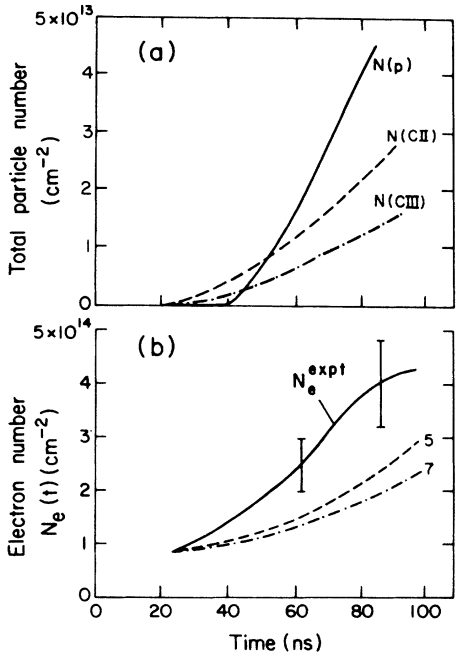

FIG. 11. (a) Calculated total number per square centimeter in the plasma of C II, C III, and protons [$N(\mathrm{C\,II},t)$, $N(\mathrm{C\,III},t)$, and $N(p,t)$, respectively] using the source functions given in Table I for 7 eV. In calculating $N(p,t)$ only protons produced by hydrogen ionization are accounted for. The uncertainties of the areal densities N with respect to each other are ±30% and the absolute uncertainty is ±50%. (b) Calculated total electron number $N_e(t)$ per square centimeter obtained from Eq. (4) together with the experimental total electron number $N_e^{\mathrm{expt}}(t)$ obtained from H_β broadening. $N_e(t)$ is given for $T_e=5$ and 7 eV as indicated, see Table I. The uncertainty in $N_e^{\mathrm{expt}}(t)$ is ±20% as indicated. The uncertainty in $N_e(t)$ is ±50%, caused by the uncertainty in the absolute particle fluxes.

Since hydrogen ionization is faster than C II ionizaton then, using the discussion in Sec. V A, the ratio between the direct proton ejection rate to that of hydrogen is expected to be approximately greater than $A(\mathrm{C\,III})/A(\mathrm{C\,II})$. Assuming equality yields a proton ejection rate that increases the calculated $N_e(t)$, bringing it to within the error bar of $N_e^{\mathrm{expt}}(t)$ shown in Fig. 11 for the entire range of T_e (5–9 eV). Thus, assuming a reasonable direct proton flux from the anode surface, the particle fluxes here determined explain the rise of the total electron density during the pulse.

C. Plasma composition

In Sec. V B we presented the total abundances of protons and carbon ions in the plasma. In this section we present the total numbers of neutral particles and other ions observed in the plasma. We use our measurements and calculations for $T_e=7$ eV (see Sec. IV) to obtain the areal densities N(H), N(C I), N(Mg I), N(Mg II), N(Al I), N(Al III), N(Ca I), and N(Ca II) as functions of time. We use the P source for Al III and the L source, that allows for continued ejection after the pulse, for the neutral particles and for Mg II and Ca II (see discussions in Sec. IV D). The results are shown in Fig. 12.

The average hydrogen concentration in the plasma ($\simeq 7\times 10^{13}$ cm^{-2}, see Table I) is about 20% of the electron density [given by N_e^{expt} in Fig. 11(b)]. The hydrogen at such a concentration does not affect the particle transport since the estimated proton hydrogen collision time is about 1 μs, and the electron-hydrogen collision time, dominated by elastic collisions,[36] is estimated to be approximately 20 ns, which is approximately 70 times longer than the electron-ion collision time.[37] The hydrogen atoms, however, contribute through ionization a significant amount of protons across the plasma, as discussed in Sec. V E.

We now discuss the ratios between the various particle fluxes. The hydrogen flux and the total C I, C II, and C III fluxes were found to be about 2000 times larger than both the total Mg I and Mg II fluxes and the total Ca I and Ca II fluxes. However, the Mg III and the Ca III fluxes (not observed in the present study) should also be taken into account. Using the ratio of C III to C II ejection rates, and estimating the C II ionization time on the dielectric surface relative to those of Mg II and Ca II, we obtain that the Mg III and Ca III fluxes into the plasma are 2–10 times larger than the Mg II and Ca II fluxes. The total flux of the carbon species would then be only about 400 times larger than the total fluxes of magnesium and calcium. We estimate that our epoxy mixture contains about ten times more carbon than magnesium or calcium atoms. This means that the flux of carbon species injected into the plasma is approximately 40 times larger than the magnesium and the calcium flux, relative to the abundance ratio in the epoxy. This presumably results from the dominant contribution of adsorbates on the surface (usually hydrocarbons and water) to the material injected into the plasma. This can be expected from the vacuum

conditions in the present experiments.

The hydrogen ejection rate is approximately 5 times larger than the total rate of C I and C II [see Table I and Fig. 12(a)]. This excessive hydrogen flux may result from excessive adsorption of water on the dielectric surface.

The total ejection rate of Mg I and Mg II was found to be twice the total of Ca I and Ca II. However, as said above, for magnesium and calcium the doubly charged ion fluxes are estimated to be significantly larger than those of the lower charge states. The Ca II ionization time in the plasma is about twice as short as that of Mg II. If we assume that the ratio between the ionization times on the surface is similar to that in the plasma, then because of the faster Ca II ionization the flux ratio of Ca III to Ca II is estimated to be about twice as large as the corresponding ratio for magnesium. Therefore, the total fluxes of magnesium and calcium particles are similar. This estimate is close to the ratio of the magnesium particle number to the calcium number ($\simeq 1.3$) in our epoxy admixture. Thus, it is consistent with particles of similar abundances in the epoxy being released in similar quantities.

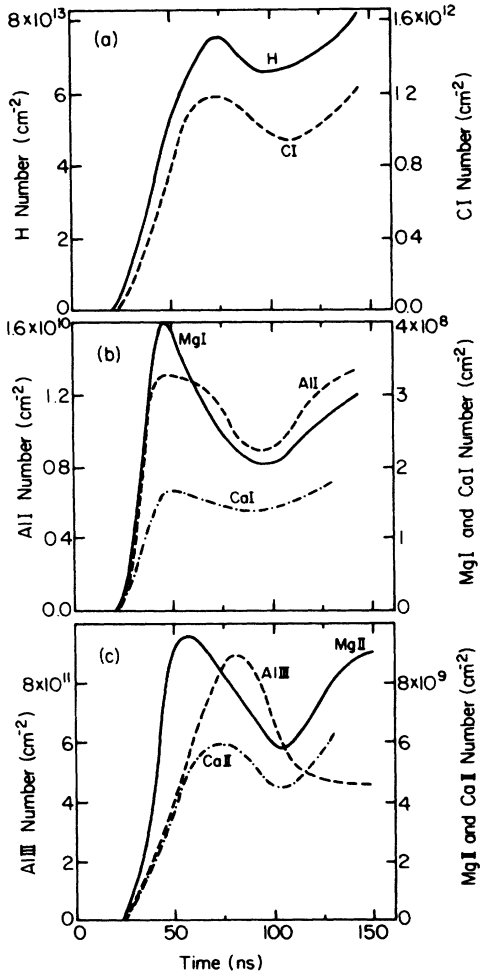

FIG. 12. Calculated total particle number N per square centimeter in the plasma obtained from the source functions determined in Sec. IV for $T_e = 7$ eV for (a) H and C I; (b) Mg I, Al I, and Ca I; and (c) Mg II, Al III, and Ca II. The relative uncertainty is ±30% and the absolute uncertainty is ±50%.

The Al I flux is about 60 times larger than the Mg I flux while the number of Al I atoms in the epoxy is half that of Mg I. The reason for this is not known to us. It cannot be explained by aluminum contribution from the aluminum ribs in the anode structure, since the aluminum flux was large also for an anode made of brass (rather than aluminum). The Al I flux is approximately 30 times smaller than the C I flux (see Tables I and II) and the Al III concentration in the plasma is about 20 times smaller than the C III concentration.

The concentrations of oxygen and nitrogen species in the plasma were not studied quantitatively. However, from the observed intensities of O II and O III lines we inferred that the O III concentration is a few times smaller than C III. This is consistent with previous measurements[10] of the composition of ion beams extracted from anode plasmas produced by surface flashover of various dielectric materials. In those experiments the oxygen ion concentration in the beam was found to be about an order of magnitude smaller than that of carbon ions. A few line intensities indicated that the nitrogen component in the plasma was smaller than that of oxygen.

D. Particle flow in the plasma

The details of the axial motion of the protons (of Larmor radius $\simeq 0.7$ mm which is about $\frac{1}{3}$ of the plasma thickness) and of the heavier ions in the plasma (Larmor radii comparable to or larger than the plasma thickness) need further studying. For the present analysis we use observations[15] of the ion velocity distribution perpendicular to the anode and of the average ion velocity away from the anode. These have been obtained for C III from measurements of the 2297-Å-line Doppler broadening and Doppler shift perpendicular to the anode surface. The observations were found to be consistent with the assumption that C III ions move away from the anode surface with the positive half of a Gaussian velocity distribution.[15] This Gaussian velocity distribution was similar to that observed parallel to the anode which corresponded to a C III temperature $T(\text{C III}) \simeq 20$ eV. The average (positive) velocity away from the anode was found to be (to within the measurement uncertainty) equal to the average of the positive half of the distribution, i.e.,

$$0.57\sqrt{2kT(\text{C III})/M(\text{C})}\ ,$$

where M(C) is the carbon mass. We, therefore, assume that the average flow of C III can be described as a ballistic motion of particles ejected from the anode surface with a Gaussian positive-velocity distribution.

Because of the weak line emission the average axial velocities of C II and C I particles could not be measured with a satisfactory accuracy. We assume that for these particles the axial velocity distributions are close to the positive half of their observed velocity distributions parallel to the anode. C I and C II are, in addition, assumed to continuously ionize as they traverse the plasma while the C III ionization is neglected due to its slow rate.

Thus, assuming a positive Gaussian-like axial velocity distribution for the C I particles ejected at the anode surface, the continuity equation gives their density as a function of time and distance from the surface,

$$n(\mathrm{C\,I},x,t)=\frac{2}{v(\mathrm{C\,I})\sqrt{\pi}}\int_0^t\frac{S(\mathrm{C\,I},t')}{t-t'}\exp\left[-\left[\frac{x/(t-t')}{v(\mathrm{C\,I})}\right]^2\right]\exp\left[-\frac{t-t'}{\tau(\mathrm{C\,I})}\right]dt' , \tag{5}$$

where $v(\mathrm{C\,I})=\sqrt{2kT(\mathrm{C\,I})/M(\mathrm{C})}=1.1$ cm/μs is the velocity of C I determined from the measured velocity distribution.[15] The flux function $S(\mathrm{C\,I},t')$ is the continuous absolute C I source determined in Sec. IV. The C I density is assumed to decrease exponentially with a time constant equal to the ionization time $\tau(\mathrm{C\,I})$ [$\tau(\mathrm{C\,I})\simeq 25$ ns for $T_e=7$ eV]. The ionization times used in the present discussion are the time-averaged ionization times obtained from the collisional-radiative calculations.

The C II density is given by

$$\begin{aligned}n(\mathrm{C\,II},x,t)=&\frac{2}{v(\mathrm{C\,II})\sqrt{\pi}}\int_0^t\frac{S(\mathrm{C\,II},t')}{t-t'}\exp\left[-\left[\frac{x/(t-t')}{v(\mathrm{C\,II})}\right]^2\right]\exp\left[-\frac{t-t'}{\tau(\mathrm{C\,II})}\right]dt'\\&+\frac{2}{v(\mathrm{C\,I})\sqrt{\pi}}\int_0^t\frac{S(\mathrm{C\,I},t')}{t-t'}\exp\left[-\left[\frac{x/(t-t')}{v(\mathrm{C\,I})}\right]^2\right]\frac{\tau(\mathrm{C\,II})}{[\tau(\mathrm{C\,II})-\tau(\mathrm{C\,I})]}\left[\exp\left[-\frac{t-t'}{\tau(\mathrm{C\,II})}\right]\right.\\&\left.-\exp\left[-\frac{t-t'}{\tau(\mathrm{C\,I})}\right]\right]dt' .\end{aligned} \tag{6}$$

The first term in the equation gives the C II density that results from the continuous source of C II, $S(\mathrm{C\,II},t')$ determined in Sec. IV. Here, $v(\mathrm{C\,II})$ and $\tau(\mathrm{C\,II})$ are the observed C II velocity ($\simeq 1.8$ cm/μs)[15] and the average C II ionization time ($\simeq 120$ ns for 7 eV). The second term gives the density of the C II ions that are produced by the C I ionization and thus have the same velocities as the C I particles. In this term the C II losses due to ionization into C III are also accounted for. The C III density is obtained similarly by calculating the C III production due to the ionizations of C I and C II, by using the C III flux, and by using $v(\mathrm{C\,III})=1.8$ cm/μs as observed.

Axial distributions of C I, C II, and C III densities obtained for $T_e=7$ eV are given in Fig. 13. It is seen that C I ionizes close to the anode surface and C II within less than 1 mm from the surface. Thus, although the plasma is fed by C I and C II, the C III ions, being negligibly ionized, dominate the outer region of the plasma. Calculation of the C III flux in this region will be given in Sec. V E 3.

The preponderance of the C III density over the C II density in the outer plasma region should be reflected in the relative current densities of these ions drawn in the diode gap. This is consistent with our experiments in which no C II line emission could be detected from the diode acceleration gap while significant line emission from C III ions was observed. It is also consistent with our charge-collector measurements (see Sec. V E 3) that showed that most of the nonprotonic ions in the beam are C III ions. Furthermore, it is consistent with mass spectroscopy data[38,11,10,13] for ions extracted from magnetically insulated diodes using surface-flashover anode plasmas. In these experiments most of the carbon ion current was carried by doubly ionized carbon atoms. Ion traces that were interpreted as C II might have resulted from charge exchange of C III ions outside the diode, as suggested by Johnson[11] and Dreike,[13] or from Al III ions which are close in charge to mass ratio to C II ions.

We believe that the picture presented here for the flow of carbon ions is also valid for the flow of the other large Larmor radii ions in the plasma. Some differences between the various species are expected due to differences in the ionization rates and the particle velocities. In general, neutral particles and singly charged ions (except for hydrogen, see Sec. V E) are ionized within less than 1 mm from the anode surface and they contribute little to the ion beam. The doubly and the triply charged ions propagate farther than the lower charge states due to their negligible ionization.

E. Hydrogen ionization in the plasma

1. Hydrogen density in the plasma

We have shown in Sec. V B that, due to ionization, hydrogen injection into the anode plasma continuously increases the plasma areal electron density. Using $\tau(H)=65$ ns for 7 eV and a kinetic energy of 8 eV for hydrogen[15] we calculate the hydrogen density distribution

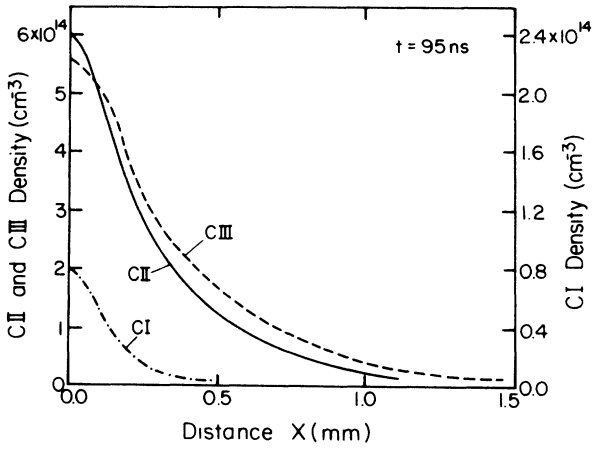

FIG. 13. Calculated axial density distributions of C I, C II, and C III for $t=95$ ns, using the P source functions determined for $T_e=7$ eV and given in Table I. The use of the L source for C I is not necessary since it little affects the C I total density for $t<95$ ns, see Table I. The relative uncertainty between C I, C II, and C III densities is $\pm 30\%$ and the absolute uncertainty is $\pm 50\%$. These uncertainties do not account for the uncertainty in T_e.

$n(H,x,t)$ as described in Sec. V D. Figure 14 shows $n(H,x)$ for $t=35$, 55, 75, and 95 ns. These density profiles demonstrate the caution required in deducing particle velocities from spatial line-intensity distributions. The "expansion" of the hydrogen profiles depends both on the hydrogen velocity and ionization time. For $t \lesssim 75$ ns the hydrogen flux close to the anode surface is relatively large, thus about offsetting the hydrogen losses due to ionization. The density profiles, therefore, are seen to expand at a velocity approximately greater than 1 cm/μs, i.e., reasonably close to the average of the positive half of the hydrogen velocity distribution parallel to the anode.[15] However, for later times ($t \gtrsim 75$ ns) and/or for larger distances from the anode surface ($x \gtrsim 0.5$ mm) the hydrogen flux is smaller, allowing the hydrogen ionization to almost prevent the expansion of the hydrogen cloud. This is shown by the similarity of the density profiles for $t=75$ and 95 ns given in Fig. 14.

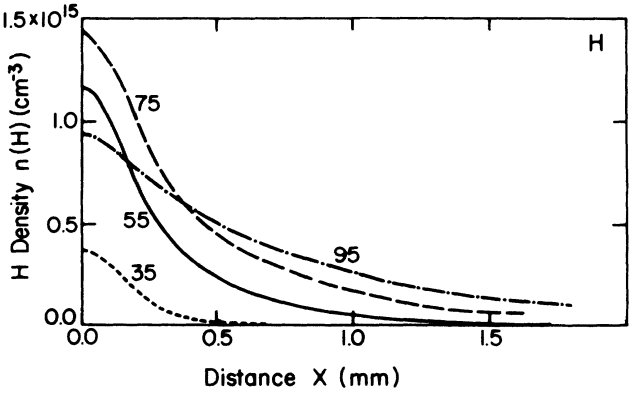

FIG. 14. Axial hydrogen density distributions $n(H,x,t)$ calculated using the P source function with $A(H)=2.5\times10^{12}$ particles/cm^2 ns obtained for $T_e=7$ eV, see Table I. Distributions are given for four times as indicated in nanoseconds. The absolute uncertainty is $\pm50\%$.

2. *Proton flux in the plasma*

The flow of the magnetized[15,16] anode plasma depends on the plasma collisionality and pressure gradient. As discussed in Refs. 14 and 15, it is possible that the anomalous plasma collisionality allows the plasma to flow at the observed rate of approximately 1 cm/μs. The proton flux in the plasma away from the anode surface is not known. In this section we discuss only the proton flux in the outer plasma region that results from the ionization of hydrogen there. For each position x_0 we calculate the hydrogen ionization within a proton Larmor radius r_p ($r_p \lesssim 0.7$ mm) near x_0, i.e., for $(x_0-r_p)<x<x_0$ mm. The proton flux through x_0, $F_p(x_0,t)$, is estimated by assuming that half of the protons produced in this region retain the hydrogen velocity until they reach x_0. The other half is assumed to turn in the magnetic field before reaching x_0. $F_p(x_0,t)$ is then given by

$$F_p(H,x_0,t)=\frac{1}{v(H)\sqrt{\pi}}\int_0^t \frac{S(H,t')}{t-t'}\exp\left[-\left[\frac{x_0/(t-t')}{v(\mathrm{H})}\right]^2\right]\exp\left[-\frac{t-t'}{\tau(\mathrm{H})}\right]\left[\exp\left[\frac{r_p(t-t')}{x_0\tau(\mathrm{H})}\right]-1\right]\frac{x_0}{t-t'}dt' \,. \tag{7}$$

In order to obtain an estimate of this proton flux in the outer plasma region we calculate $F_p(x_m,t)$, where x_m is the farthest position for which the electron density was measured [see Fig. 4(a)], although the electric-field-excluding plasma perhaps extends beyond x_m. $F_p(t)$ for $x_m=1.5$ mm and for $T_e=5$ and 7 eV is shown in Fig. 15(a).

The hydrogen continuous supply causes the proton flux at $x_m=1.5$ mm to rise in time. At the end of the pulse ($t\simeq95$ ns) it becomes $\simeq10^{20}$ cm^{-2}s^{-1} which is about 20% of the total current density drawn from the plasma at that time (80–100 A/cm^2). It is approximately greater than 50% of the proton current density since at this time the proton fraction in the ion beam was found to be about 30% [see below in Fig. 15(c)]. Thus, it is possible that the proton fraction in the extracted ion beam is significantly affected by hydrogen ionization in the outer plasma region rather than by the flow of the magnetized protons from the vicinity of the anode surface.

Clearly, neutral particles other than hydrogen contribute must less ions than hydrogen in the outer plasma region due to their lower velocity, shorter ionization time, and smaller flux into the plasma. For example, repeating this calculation for C I gives a C II flux about 300 times smaller than the proton flux.

We note that the hydrogen atoms in the plasma are expected to undergo charge-exchange collisions with the protons. In our plasma the mean free path of hydrogen for such collisions is slightly greater than 2 mm (Ref. 39) (assuming that protons constitute half of the positive charge in the plasma, see Table I), thus these collisions were neglected in the present analysis. For higher plasma densities these charge-exchange collisions may affect more the proton flux, since the charge-exchange collision rate would increase with the proton density.

3. *Implication for the proton to C III ratio in the ion beam*

In this section we shall use the calculated C III density profiles (see Sec. V D) to obtain the C III flux in the outer plasma region. The C III flux at the point x_0 is obtained by multiplying the integrands in the continuity equation for C III by the velocity factor $x_0/(t-t')$. $F(\mathrm{C\,III},t)$ was calculated for $T_e=5$ and 7 eV using the corresponding source amplitudes (see Table I) and ionization times. $F(\mathrm{C\,III},t)$ for $x_0=x_m=1.5$ mm, obtained for $T_e=5$ and 7 eV, is compared in Fig. 15(a) to the proton flux $F_p(t)$. The C III flux starts rising later than the proton flux because of the lower velocity of C III. However, due to the continuous increase in the density of the nonionizing C III

ions, their flux rises faster than that of the protons and it becomes similar to the proton flux at the end of the pulse ($t \simeq 95$ ns). This is seen more clearly in Fig. 15(b) where the calculated ratio between the C III and the proton flux is shown for $x_0 = 1.5$ mm for $T_e = 5$ and 7 eV. The total of C III and proton fluxes for $x_0 = 1.5$ mm given in Fig. 15(a) at the end of the pulse is about half the ion current density ($\lesssim 100$ A/cm^2) drawn from the plasma at this time. Therefore, to within the uncertainties, the flux ratios given in Fig. 15(b) are expected to cause the C III to proton flux ratio in the ion beam to rise in time during the pulse. The calculated ratio between the C III charge flux and the total charge flux,

$$R = 2eF(\text{C III},t)/[2eF(\text{C III},t)+eF_p(t)] ,$$

for $T_e = 5$ and 7 eV is plotted in Fig. 15(c).

In Fig. 15(c) we also present the observed time-dependent fraction of the heavier-than-proton ions in the extracted ion beam. The latter is denoted by J_h/J_i, where J_h is the heavy-ion current density and J_i is the total ion current density. It is obtained from charge-collector measurements using negatively biased magnetically insulated collectors covered and not covered by a 2-μm-thick polyethylene foil that lets through only protons above approximately 180 keV. The charge collectors were mounted 4 cm behind the cathode to reduce ion time-of-flight effects, thus allowing the time dependence of J_h/J_i to be obtained. In order to examine whether most of the heavy ions in the beam are C III ions, we also used collectors at a distance of 90 cm from the diode. We obtained two clear ion signals, separated due to time-of-flight effects, that corresponded to protons and C III. The uncertainties allowed us to conclude that the ratio of the C III to proton time-integrated signals in this measurement was at least half the ratio obtained from the charge collectors placed 4 cm behind the cathode [given in Fig. 15(c)], averaged over time. This is consistent with our prediction, discussed in Sec. V D, that a significant fraction of the nonprotonic ions in the beam is C III ions. The separated C III and proton signals obtained from the far collectors were also used to verify that the 2-μm-thick foil stopped the C III ions while passing most of the protons.

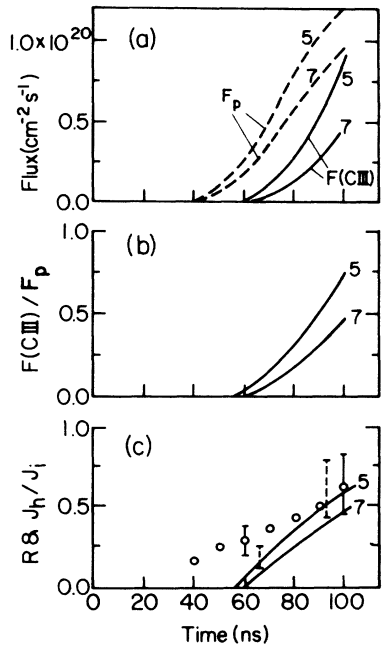

FIG. 15. (a) The proton flux $F_p(x_0,t)$ [see Eq. (7)] and the C III flux $F(\text{C III},x_0,t)$ as a function of time for $x_0 = 1.5$ mm and for $T_e = 5$ and 7 eV as indicated. For each T_e we used the corresponding source amplitudes (see Table I) and the calculated ionization times. The absolute uncertainty in $F_p(x_0,t)$ and $F(\text{C III},x_0,t)$ is $\pm 50\%$. (b) Ratios of C III to proton fluxes for $T_e = 5$ and 7 eV as indicated. The uncertainty for each T_e is $\pm 40\%$. (c) The fraction of the C III charge flux $R = 2F(\text{C III})/[2F(\text{C III})+F_p]$ for $T_e = 5$ and 7 eV as indicated for $x_0 = 1.5$ mm. The uncertainty is $\pm 30\%$ as shown by the dashed error bars. Also shown is the measured ratio J_h/J_i of the nonprotonic ion current to the total current obtained from charge-collector measurements. The points are averages of two collectors placed 1 cm below and above the ion beam center 4 cm behind the cathode. The difference between the collectors and the shot-to-shot repeatability were within the indicated uncertainty of $\pm 30\%$.

We can now compare the calculated fraction R of the C III charge flux in the outer plasma region to the C III fraction in the ion beam (which is similar to J_h/J_i), as shown in Fig. 15(c). The temporal rise of R is similar to the rise of J_h/J_i late in the pulse. However, J_h/J_i is observed to be larger early in the pulse. Early in the pulse J_h/J_i is probably determined by the relative particle density distributions in the plasma after its formation (as shown in Sec. V B, the total plasma areal density at $t = 25$ ns is $\simeq 10^{14}$ particles/cm^2 which is sufficient to provide about three times the ion current extracted over the entire pulse). The similar rise of the calculated charge flux R late in the pulse to that of the observed J_h/J_i suggests that the motion and ionization of particles injected from the anode surface affect the relative extracted fluxes in this period of time. It appears that the proton and the C III fluxes (for protons due to hydrogen ionization and for C III due to the ballistic motion with the observed Gaussian velocity distribution) may significantly affect the relative particle densities in the ion-emitting region of the plasma. As already mentioned, however, the particle density distribution is also affected by the plasma flow due to the plasma pressure gradient.

This analysis also shows the dependence of the relative particle fluxes in the outer plasma region on the plasma thickness. The thinner the plasma the larger the relative heavy-ion fluxes in the outer region early in time. For thicker plasmas the protons dominate at early times due to the relatively fast hydrogen motion. However, at later times the fraction of doubly charged ions in the ion flux will become larger than for thinner plasmas due to the axial decay of the hydrogen density as a result of its ionization. The relative particle fluxes are also sensitive to the plasma parameters. For example, for moderately higher electron densities the C III ionization time is still relatively long but the hydrogen ionization time becomes significantly shorter. This will reduce the hydrogen density away from the anode surface with the C III density remaining the same.

Johnson and coworkers,[38] in their experiments with applied-B-field ion diodes using surface-flashover anode

plasmas, observed the ion beam to be composed of $\gtrsim 75\%$ proton current for the first 20 ns of the pulse, but with increasing amounts of highly ionized carbon species later in time. This can be qualitatively explained by our results [see Fig. 15(b)] which predict a continuous rise of the C III to proton flux ratio in the outer region of the plasma.

As shown here the relative fluxes of various ions extracted from plasmas vary in time and depend on the relative particle densities, particle velocities, plasma electron density, plasma temperature, and plasma thickness. This sensitivity is perhaps the reason for the diversity (30–80 %) in the proton fraction observed[11–13] in ion beams extracted from diode configurations that are similar to each other, in which surface-flashover anode plasmas were used.

4. *Hydrogen flow into the diode acceleration gap*

Hydrogen atoms that remain neutral as they traverse the anode plasma are expected to stream into the diode acceleration gap. Using the continuity equation for hydrogen, these atoms are estimated to fill the diode gap during the pulse with a density of 10^{12}–10^{13} cm^{-3}. Neutral particles with such densities have no effect on the diode operation since they negligibly collide with the accelerated particles. In principle, they can cause the production of fast neutral particles via charge exchange collisions with the ions accelerated in the gap (the fast neutral particles will have up to approximately 10 keV energy because of the energy dependence of the cross section[39]). Such a process has been suggested by Prono and coworkers[40] for their reflex-ion diodes. However, in the present experiment this effect is small due to the low neutral-layer density. The fast neutral-particle flux is estimated (using a proton-hydrogen charge-exchange collision cross section of 2×10^{-15} cm^2)[39] to be approximately 1% of the ion flux, thus filling the diode with about 10 keV neutral particles by less than one-tenth of the ion density (i.e., $\simeq 10^{11}$ cm^{-3}). In diodes in which the electron temperature is lower a larger fraction of neutral hydrogen will reach the outer plasma region. The resulting larger neutral-particle density over the anode plasma may result in a more significant production of fast neutral particles.

F. Electron energy losses in the plasma

Knowledge of the plasma composition allows us to estimate the electron energy losses in the plasma and to compare them with our previously estimated[14] electron heating. The main energy-loss mechanisms for the electrons are ionization and excitation of the plasma particles (free-free transitions are negligible for the present parameters[1]).

The average total energy loss $L_{\rm ion}(k)$ per electron, due to the ionization of a species k during the entire pulse (where we take the end of the P source at $t=t_0+76=96$ ns as the end of the pulse), is calculated by

$$L_{\rm ion}(k)=\frac{l_x}{N_e}\int_{t_0}^{t_0+76}[E(k)+\tfrac{3}{2}T_e]\times\left[\sum_j S_j(k,t)n_j(k,t)\right]dt\ , \quad (8)$$

where $E(k)$, $S_j(k,t)$, $n_j(k,t)$, and N_e are the ionization potential, the time dependent ionization rate from the level j, the density of the level j, and the number of electrons per square centimeter. Here, the ionization potential $E(k)$ from the ground state is used since all free electrons produced originate from the ground state. The energy $\frac{3}{2}T_e$ required to give the newly released electron the mean electron kinetic energy is also accounted for. For N_e we use 2.5×10^{14} cm^{-2} which is an average of $N_e^{\rm expt}(t)$ over the pulse [see Fig. 11(b)]. The decrease in the electron temperature due to ionization, $\Delta T_e^{\rm ion}(k)=(\frac{2}{3})L_{\rm ion}(k)$, is given in Table III for the major plasma

TABLE III. Electron cooling during the entire pulse (up to $t=96$ ns) calculated for $T_e=5$ and 7 eV using the corresponding source functions given in Table I for C I, C II, C III, and H particles. $\Delta T_e^{\rm ion}(k)$ and $\Delta T_e^{ex}(k)$ are the values of the electron cooling due to ionizations and impact excitations obtained from Eqs. (8) and (10), respectively. Also given are the values of the total cooling ΔT_e for the two temperatures. The uncertainties are mainly due to the uncertainty in the absolute particle areal densities.

Species	T_e (eV)	Ionization Cooling $\Delta T_e^{\rm ion}(k)$ (eV) (±50%)	Radiation Cooling $\Delta T_e^{ex}(k)$ (eV) (±50%)	Total Cooling ΔT_e (eV) (±50%)
C I	5	0.10	<0.01	0.10
	7	0.26	<0.01	0.26
C II	5	0.27	2.0	2.3
	7	0.86	1.4	2.3
C III	5	0.01	2.9	2.9
	7	0.01	0.7	0.70
H	5	2.4	0.21	2.6
	7	2.7	0.24	2.9
Total	5			7.9
	7			6.2

components (C I, C II, C III,and H) for $T_e=5$ and 7 eV. The numbers for $T_e=9$ eV are very similar to those for 7 eV. Hydrogen ionization dominates the electron cooling due to the relatively high hydrogen density and ionization rate.

The net energy losses due to excitations can be estimated from the total line emission that escapes from the plasma. The total radiation losses $L_r(k)$ per cm^2 for each species k during the entire pulse are given by

$$L_r(k)=l_x\int_{t_0}^{t_0+76}\left[\sum_{u,l} n_u(k,t)A_{ul}E_{ul}\right]dt\ , \tag{9}$$

where $n_u(k,t)$, A_{ul}, and E_{ul} are the population of the level u of the species k, the Einstein coefficient for the transition from the level u to the level l, and the energy of the emitted photon. For the thick lines we used the appropriate escape factors as discussed in Ref. 14, but the mild optical thickness effects had little influence on the estimate of $L_r(k)$. The total energy loss $L_{ex}(k)$ per electron during the pulse due to impact excitations of the species k is obtained by

$$L_{ex}(k)=L_r(k)/N_e\ . \tag{10}$$

The corresponding decrease in the electron temperature $\Delta T_e^{ex}(k)=(\frac{2}{3})L_{ex}(k)$ is presented in Table III, showing that the electron cooling due to impact excitations is dominated by C II and C III excitations.

The total electron cooling is given in the last column in Table III. When summed over all loss channels it amounts to $\Delta T_e\simeq 7$ eV, and it is not sensitive to the electron temperature within our uncertainty range. It is suggested in Ref. 14 that this electron cooling, together with the smaller energy loss due to thermal convection to the anode surface, about balances the Ohmic electron heating dominated by the pressure-driven currents in the plasma. We note that an additional term of the electron energy loss results from the excitation of particles supplied at their ground state to the final population distribution at the end of the pulse. However, this contribution is much smaller than $L_{\rm ion}(k)$ and $L_{ex}(k)$ since ionizations and radiative decays are fast compared to the length of the diode pulse. Also, in this discussion we ignored the flow of electrons to and from the anode surface. This is equivalent to assuming that the energy of electrons that flow into and out of the plasma is on the average similar to the electron thermal energy.

G. Further comparison with previous studies and possible use in plasma source design

The relation between the hydrogen $n=3$ level population and the proton density should be emphasized. Due to the continuous hydrogen source, partial local thermodynamic equilibrium (LTE) for the hydrogen levels does not exist even though the time required for the $n=3$ level to reach partial LTE with the proton state for an ionized plasma, of the present density and temperature, is very short, approximately 0.2 ns (see discussion by Griem[1] on rapidly ionizing plasmas). Thus, inferring proton densities from hydrogen line intensities should be made with caution. For example, relying on partial LTE, Hinshelwood[41] calculated the proton density from his measured H_α line intensity in the cathode plasma in a pulsed electron diode. He obtained a proton density higher than the observed one by about an order of magnitude. This discrepancy might have resulted from a possible continuous hydrogen supply to the cathode plasma in a manner similar to that described here. In our case, accounting for the continuous hydrogen source using the time-dependent collisional radiative calculations, yields a density ratio between the hydrogen $n=3$ level and the protons that is about 1000 times larger than the ratio corresponding to partial LTE. This large ratio, together with the observed H_α intensity, gives a satisfactory prediction of the proton density in the plasma (see Sec. V B).

Using ion-mass spectrometry, Johnson and coworkers[11] have found that the ion beam generated by their magnetically insulated diode (powered by a 700-kV, 300-kA, 100-ns pulse) contained about equal amounts of C III and C IV ions. They used a surface-flashover anode plasma of density 4×10^{16} cm^{-3}. We attempt to explain their result by calculating the time-dependent ionization rates of C I, C II, C III, and C IV for their plasma density. We assume that $T_e=7$ eV and that C I and carbon ions at the ground state are continuously ejected from the anode surface. Due to the relatively high electron density, C I and C II ionize in a few nanoseconds, C III ionize in tens of nanoseconds, and the C IV ionization is negligible on this time scale. The ratio of C IV to C III density rises in time and reaches unity about 50 ns after the particle ejection. Assuming a kinetic energy of 20 eV for C III (a velocity of approximately 2 cm/μs, similar to our observed[15] value), the outer region of the about 1-mm-thick anode plasma[11] will contain mostly carbon ions that have resided in the plasma for about 50 ns. Thus, the C IV to C III density ratio would be close to 1 in the outer plasma region in agreement with the ratio found in the beam. Clearly, the thicker the plasma (for the same plasma density and temperature) the more will the C IV ions dominate the plasma front.

The analysis given here and in Sec. V E shows that investigating the particle velocity distributions and the ionization processes as a function of time and position in pulsed plasma sources may help control the charge-state distribution and the proton component in the plasma front. This may be important for the design of plasma sources for various plasma injection experiments.

VI. SUMMARY

Using absolute line intensities measured as a function of time we determined the absolute time-dependent injection rates of various atoms and ions from the dielectric anode surface into the anode plasma in a magnetically insulated ion diode. For this determination, time-dependent collisional-radiative calculations of the atomic level populations, based on experimentally determined electron temperature and density, were used.

Neutral particles, singly charged ions, and doubly charged ions were found to continuously stream from the surface into the plasma during the diode voltage pulse.

The efficiency of ejection of particles like magnesium and calcium that were admixed to the epoxy was at least an order of magnitude smaller than that of hydrogen and carbon. The processes that govern the material ejection from the surface and the time dependence of the particle fluxes are not known and no attempt was made by us to investigate them. However, the data suggest that ionization processes in the immediate vicinity of the anode surface produce singly and doubly charged ions. The higher the ionization rate of a certain species on the surface, the larger the flux of the ionization product. These observations, together with measurements of the kinetic energies of various ions in the plasma, allowed us to infer that the higher the charge state of a particle produced on the surface the larger its kinetic energy after ejection. Presumably, this results from electric fields on the surface, consistent with the observation[15] that the ions acquire their kinetic energies in the immediate vicinity of the anode surface. The rise of the total plasma areal density was found to be determined by the continuous material ejection (mainly H, C I, C II, and C III for the present plasma) from the anode surface.

The ejection of neutral particles continued also after the diode voltage pulse when the applied electric field was low. However, the ejection of doubly charged ions was found to drop sharply after the pulse, perhaps due to a reduction in the ionization rates of the singly charged ions on the surface at this period. This is consistent with the finding that the ejection of singly charged ions (Mg II and Ca II) of elements of relatively fast ionizing neutral particles continued. In contrast, the ejection of C II ions decreased at late times, presumably due to the relatively slow C I ionization on the anode surface.

Using the presently determined time-dependent particle fluxes, the particle velocity distributions (observed from line Doppler broadening[15]), and the particle ionization times (determined from the observed electron temperature,[14] electron density,[15] and time-dependent collisional-radiative calculations) we calculated the density distributions of neutral particles and ions as a function of time and distance from the anode surface. The calculations predict that mainly doubly charged ions (mostly C III ions for the present plasma) and protons dominate the outer (ion-emitting) region of the plasma, consistent with measurements on the extracted ion beam. Hydrogen ionization in the outer plasma region produces a proton flux about half the proton current density drawn from the plasma. The proton flux due to the hydrogen ionization can be important if the flow of magnetized protons in the plasma is slow. The calculated rise in the flux ratio between C III ions and protons in the outer plasma region was found to be consistent with the rise of the current-density ratio for these particles determined from charge-collector measurements outside the diode. The domination of the plasma outer region by doubly charged ions and the rise of C III to proton flux ratio during the pulse are consistent with charge-collector measurements on the extracted ion beams reported in previous studies.[10,11,13,38]

The determination of the plasma composition allowed us to obtain the electron energy losses due to inelastic collisions, mainly with H, C II, and C III. These energy losses dominate the electron cooling in the plasma and, together with the estimated electron thermal convection to the anode surface, about balance the Ohmic heating caused by the pressure-driven current in the plasma.[14]

Using time-dependent calculations we showed (see Secs. IV E and V G) that for this plasma in a pulsed diode, and probably for plasmas in many pulsed power systems, estimates of the density of the charge state z from the populations of the density of high levels of the charge state $z-1$ can be erroneous by 2–3 orders of magnitude, even though the criterion[1] for the establishment of partial local thermal equilibrium is well fulfilled. This results from the continuous material flow into the plasma observed here and from the transient nature of the ionization processes.[1]

The electron density and temperature together with the material ejection from surfaces into the plasma determine the plasma density profile and particle charge states. In order to achieve better control of these processes further quantitative observations with varying parameters must be performed. For example, different surface conditions and surface coatings, metal-dielectric structures, diode currents, and voltages may be used. Ion-mass spectrometry of ion beams, as done by many authors,[10,11,13] coupled with spectroscopic investigations of the anode plasma, may provide further insight into the processes that dominate ion extraction from plasmas under strong electric and magnetic fields. Investigations of time-dependent spatial density distributions of different ions and charge states, similar to the ones presented here (see results and discussion in Secs. V D, V E, and V G), may be helpful in the design of plasma sources for various applications. We believe that the presently developed diagnostic tools are suitable for investigation of plasmas in a variety of important pulsed power systems.

Finally, such quantitative studies of the release and ionization of particle species on surfaces can be used in investigating the mechanisms involved in electrical breakdown of dielectric surfaces. They may also be helpful in studying problems related to plasma wall interaction.

ACKNOWLEDGMENTS

The authors gratefully acknowledge A. E. Blaugrund, Z. Zinamon, and H. R. Griem for valuable discussions and critical reading of the manuscript. We are indebted to M. Markovits for the absolute calibration of the spectroscopic system, and to C. Litwin, E. Nardi, A. Fisher, and C. Mendel for stimulating remarks. Thanks are due to E. Elias for help in the data analysis and to P. Meiri and Y. Danino for skilled technical assistance.

[1]H. R. Griem, *Plasma Spectroscopy* (McGraw-Hill, New York, 1964).

[2]P. Dreike, C. Eichenberger, S. Humphries, and R. N. Sudan, J. Appl. Phys. **47**, 85 (1976); S. Humphries, Jr., Nucl. Fusion **20**, 1549 (1980).

[3]J. P. VanDevender, Plasma Phys. Controlled Fusion **28**, 841 (1986).

[4]G. Yonas, in *Proceedings of the International Atomic Energy Agency Meeting on Advances in Inertial Confinement Fusion Research, Kobe, Japan, 1983,* edited by C. Yamanaka (Institute of Laser Engineering, Osaka University, Osaka, Japan, 1983), p. 307.

[5]See, for example, J. M. Finn and R. N. Sudan, Nucl. Fusion **22**, 1443 (1982).

[6]R. T. Hodgson, J. E. E. Baglin, R. Pal, J. M. Neri, and D. A. Hammer, Appl. Phys. Lett. **37**, 187 (1980).

[7]M. A. Sweeney, J. E. Brandenburg, R. A. Gerber, D. J. Johnson, J. M. Hoffman, P. A. Miller, J. P. Quintenz, S. A. Slutz, and K. W. Bieg, in *Proceedings of the Fifth International Conference on High Power Particle Beams, CONF-830911, San Francisco, 1984,* edited by R. J. Briggs and A. J. Toepfer (Lawrence Livermore National Laboratory, Livermore, CA, 1984), p. 203.

[8]D. J. Johnson, J. P. Quintenz, and M. A. Sweeney, J. Appl. Phys. **57**, 794 (1985).

[9]J. M. Neri, D. A. Hammer, G. Ginet, and R. N. Sudan, Appl. Phys. Lett. **37**, 101 (1980).

[10]K. W. Bieg, E. J. T. Burns, J. N. Olsen, and L. R. Dorrell, J. Vac. Sci. Technol. A **3**, 1234 (1985).

[11]D. J. Johnson, E. J. T. Burns, J. P. Quintenz, K. W. Bieg, A. V. Farnsworth, Jr., L. P. Mix, and M. A. Palmer, J. Appl. Phys. **52**, 168 (1981).

[12]D. J. Johnson, R. J. Leeper, W. A. Stygar, R. S. Coats, T. A. Mehlhorn, J. P. Quintenz, S. A. Slutz, and M. A. Sweeney, J. Appl. Phys. **58**, 12 (1985).

[13]P. L. Dreike, E. J. T. Burns, S. A. Slutz, J. T. Crow, D. J. Johnson, P. R. Johnson, R. J. Leeper, P. A. Miller, L. P. Mix, D. B. Seidel, and D. F. Wenger, J. Appl. Phys. **60**, 878 (1986).

[14]Y. Maron, M. Sarfaty, L. Perelmutter, O. Zahavi, M. E. Foord, and E. Sarid, Phys. Rev. A **40**, 3240 (1989); Y. Maron, E. Sarid, L. Perlemutter, M. E. Foord, O. Zahavi, M. Sarfaty, C. Litwin, and E. Nahshoni, in *Proceedings of the Seventh International Conference on High Power Particle Beams, Karlsruhe, West Germany, 1988,* edited by Walter Bauer and Winfried Schmidt (Kernforschungszentrum Karlsruhe, Karlsruhe, West Germany, 1988), p. 57.

[15]Y. Maron, E. Sarid, O. Zahavi, L. Perelmutter, and M. Sarfaty, Phys. Rev. A **39**, 5842 (1989).

[16]Y. Maron, E. Sarid, E. Nahshoni, and O. Zahavi, Phys. Rev. A **39**, 5856 (1989).

[17]P. S. Ganas, Physica **104C**, 411 (1981).

[18]D. Pequignot and S. Aldrovandi, Astron. Astrophys. **50**, 141 (1976).

[19]Y. Itikawa, S. Hara, T. Kato, S. Nakazaki, M. S. Pindzola, and D. H. Crandall, At. Data Nucl. Data Tables **33**, 149 (1985).

[20]D. E. Post and R. V. Jensen, At. Data Nucl. Data Tables **20**, 434 (1977).

[21]W. L. Wiese, M. W. Smith, and B. M. Glennon, *Atomic Transition Probabilities,* Natl. Bur. Stand. Ref. Data Ser., Natl. Bur. Stand. (U.S.) Circ. No. 4 (U.S. GPO, Washington, D.C., 1966); W. L. Wiese, M. W. Smith, and B. M. Miles, *Atomic Transition Probabilities,* Natl. Bur. Stand. Ref. Data Ser., Natl. Bur. Stand. (U.S.) Circ. No. 22 (U.S. GPO, Washington, D.C., 1969).

[22]W. L. Wiese and G. A. Martin, *Wavelengths and Transition Probabilities for Atoms and Atomic Ions,* Natl. Bur. Stand. Ref. Data Ser., Natl. Bur. Stand. (U.S.) Circ. No. 68 (U.S. GPO, Washington, D.C., 1980), Part II.

[23]R. D. Cowan (private communication).

[24]R. D. Taylor and A. W. Ali, J. Quant. Spectrosc. Radiat. Transfer **36**, 373 (1986).

[25]B. C. Fawcett, At. Data Nucl. Data Tables **30**, 423 (1984).

[26]G. A. Victor, R. F. Stewart, and C. Laughlin, Astrophys. J. Suppl. Ser. **31**, 237 (1976).

[27]C. Mendoza and C. J. Zeippen, Astron. Astrophys. **179**, 339 (1987).

[28]A. Lindgard and S. E. Nielsen, At. Data Nucl. Data Tables **19**, 533 (1977).

[29]L. C. Johnson, Astrophys. J. **174**, 227 (1972).

[30]J. F. Williams, J. Phys. B **14**, 1197 (1981); R. L. Long, D. M. Cox, and S. J. Smith, J. Res. Natl. Bur. Stand. **72**, 521 (1968).

[31]M. Finkenthal *et al.*, Astrophys. J. **313**, 920 (1987).

[32]K. A. Berrington, J. Phys. B **18**, L395 (1985).

[33]J. Lang, J. Phys. B **16**, 3907 (1983).

[34]J. Lang, R. A. Hardcastle, R. W. P. McWhirter, and P. H. Spurrett, J. Phys. B **20**, 43 (1987).

[35]See, for example, E. W. Gray, J. Appl. Phys. **58**, 132 (1985), and references therein.

[36]S. Chandrasekhar and F. H. Breen, Astrophys. J. **103**, 41 (1946).

[37]L. Spitzer, Jr., *Physics of Fully Ionized Gases* (Wiley, New York, 1962).

[38]D. J. Johnson, A. V. Farnsworth, Jr., D. L. Fehl, R. J. Leeper, and G. W. Kuswa, J. Appl. Phys. **50**, 4524 (1979).

[39]See R. L. Freeman and E. M. Jones, National Service Information Service Document No. CLM-R137 (United Kingdom Atomic Energy Authority Research Group Report) (1975), Fig. 29. Copies may be ordered from the National Technical Information Service, Springfield, VA 22161.

[40]D. S. Prono, H. Ishizuka, E. P. Lee, B. W. Stallard, and W. C. Turner, J. Appl. Phys. **52**, 3004 (1981).

[41]D. Hinshelwood, Naval Research Laboratory Memo, Report No. 5492, 1985 (unpublished).